Article

Molecular Cell

LIN41 Post-transcriptionally Silences mRNAs by Two Distinct and Position-Dependent Mechanisms

Graphical Abstract

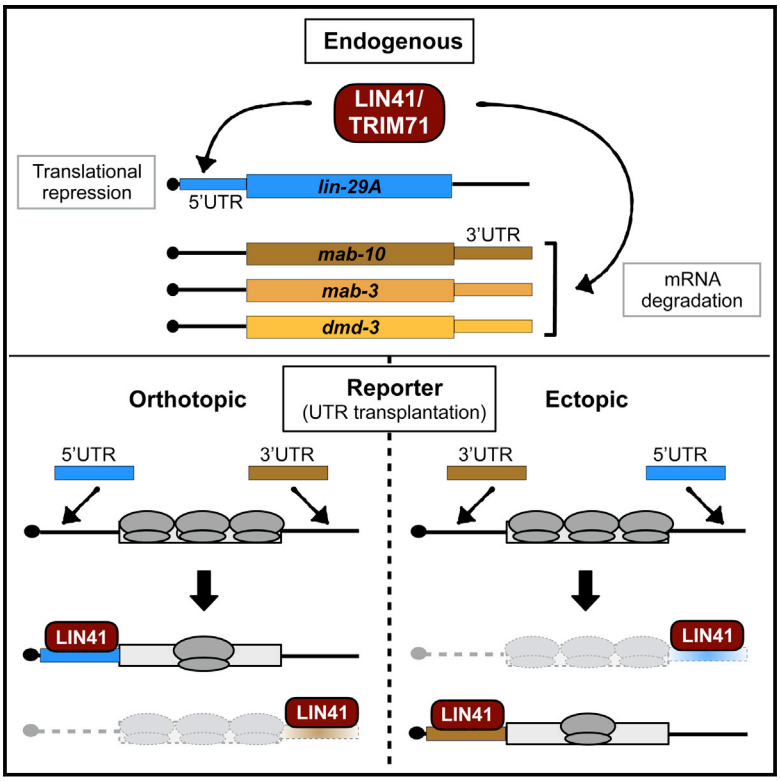

Highlights

- Ribosome profiling and RNA immunoprecipitation identify direct targets of LIN41
- Three mRNAs undergo LIN41-dependent decay, one undergoes pure translational repression
- The location of LIN41 binding on the mRNA determines the choice of mechanism
- LIN-29A/EGR and MAB-10/NAB may be evolutionarily conserved LIN41 targets

Authors

Florian Aeschimann, Pooja Kumari, Hrishikesh Bartake, Dimos Gaidatzis, Lan Xu, Rafal Ciosk, Helge Großhans

Correspondence

helge.grosshans@fmi.ch

In Brief

Aeschimann et al. report that the stem cell fate regulator LIN41 silences mRNAs through two distinct and separable mechanisms, translational repression or degradation. Choice of mechanism is specified by the location of the LIN41-binding site on the target mRNA.

Aeschimann et al., 2017, Molecular Cell *65*, 476–489
February 2, 2017
http://dx.doi.org/10.1016/j.molcel.2016.12.010

CellPress

Molecular Cell
Article

LIN41 Post-transcriptionally Silences mRNAs by Two Distinct and Position-Dependent Mechanisms

Florian Aeschimann,[1,2] Pooja Kumari,[1] Hrishikesh Bartake,[1,2] Dimos Gaidatzis,[1,3] Lan Xu,[1] Rafal Ciosk,[1] and Helge Großhans[1,4,*]

[1]Friedrich Miescher Institute for Biomedical Research, Maulbeerstrasse 66, 4058 Basel, Switzerland
[2]University of Basel, Faculty of Science, 4056 Basel, Switzerland
[3]Swiss Institute of Bioinformatics, 4058 Basel, Switzerland
[4]Lead Contact
*Correspondence: helge.grosshans@fmi.ch
http://dx.doi.org/10.1016/j.molcel.2016.12.010

SUMMARY

The RNA-binding protein (RBP) LIN41, also known as LIN-41 or TRIM71, is a key regulator of animal development, but its physiological targets and molecular mechanism of action are largely elusive. Here we find that this RBP has two distinct mRNA-silencing activities. Using genome-wide ribosome profiling, RNA immunoprecipitation, and in vitro-binding experiments, we identify four mRNAs, each encoding a transcription factor or cofactor, as direct physiological targets of *C. elegans* LIN41. LIN41 silences three of these targets through their 3′ UTRs, but it achieves isoform-specific silencing of one target, *lin-29A*, through its unique 5′ UTR. Whereas the 3′ UTR targets *mab-10*, *mab-3*, and *dmd-3* undergo transcript degradation, *lin-29A* experiences translational repression. Through binding site transplantation experiments, we demonstrate that it is the location of the LIN41-binding site that specifies the silencing mechanism. Such position-dependent dual activity may, when studied more systematically, emerge as a feature shared by other RBPs.

INTRODUCTION

Proper formation and homeostasis of tissues and organs requires switching of stem and progenitor cells from self-renewal to an appropriate differentiation program in the right place and at the correct time. Post-transcriptional mechanisms, although less well studied than contributions of transcriptional control, have been argued to play a dominant role in regulating stem cell fates (Wright and Ciosk, 2013; Ye and Blelloch, 2014). LIN41 and its regulator, the microRNA (miRNA) *let-7*, appear to have major and conserved functions in these processes. They control proliferation versus differentiation decisions not only in *C. elegans* seam cells (Reinhart et al., 2000; Slack et al., 2000), epidermal blast cells considered an in vivo stem cell model (Brabin and Woollard, 2012; Joshi et al., 2010), but also in mammalian embryonic stem cells and during human fibroblast in vitro reprogramming (Chang et al., 2012; Chiu et al., 2014; Rehfeld et al., 2015; Rybak et al., 2009; Worringer et al., 2014). It has therefore been speculated that the regulation of LIN41 by *let-7* constitutes an ancient control mechanism for self-renewal, differentiation, and cell fate plasticity in diverse tissues (Ecsedi and Großhans, 2013). Moreover, LIN41 is the one key target of *let-7* in *C. elegans* whose regulation ensures proper vulval development and, thus, viability (Ecsedi et al., 2015).

The molecular mechanisms by which LIN41 (also called TRIM71 in mammals) exerts its functions are not well understood. As a member of the TRIM-NHL protein family, post-transcriptional or post-translational mechanisms are likely (Tocchini and Ciosk, 2015). This is because the eponymous *tri*partite *m*otif of RING, B-Box, and coiled-coil domains is characteristic of proteins with E3 ubiquitin ligase activity (Ikeda and Inoue, 2012), whereas the C-terminal NHL (NCL-1, HT2A2, and LIN-41) repeat domain may mediate sequence-specific RNA binding (Loedige et al., 2015). A protein ubiquitylation activity has been established for mouse LIN41 in some contexts (Chen et al., 2012; Rybak et al., 2009), but, as *C. elegans* and *D. melanogaster* LIN41 may lack this activity (Löer et al., 2008; Tocchini et al., 2014), this seems not to account for a mechanistically conserved self-renewal activity across animal phylogeny. By contrast, LIN41 may have a conserved function in mRNA silencing. A role for LIN41 in translational repression of mRNAs was first proposed more than 15 years ago in *C. elegans* (Slack et al., 2000) and since then has been suggested repeatedly in diverse systems (Loedige et al., 2013; Spike et al., 2014b; Worringer et al., 2014). However, this notion has not been tested explicitly, but it was deduced from the observation that certain LIN41 target reporters change more extensively at the level of reporter protein activity than mRNA level (Loedige et al., 2013). Indeed, extensive evidence supports a function of LIN41 in destabilizing target mRNAs (Chang et al., 2012; Loedige et al., 2013; Mitschka et al., 2015), even in cases where this RNA-binding protein (RBP) was concluded to act by translational repression (Worringer et al., 2014).

Progress toward understanding the mode of action of LIN41 has suffered from limited knowledge of physiological LIN41 targets. In *C. elegans*, genetic interactions link CDC-25.3, a meiotic regulator (Spike et al., 2014a), and LIN-29, a transcription factor that regulates seam cell self-renewal and differentiation (Ambros and Horvitz, 1984; Rougvie and Ambros, 1995; Slack et al.,

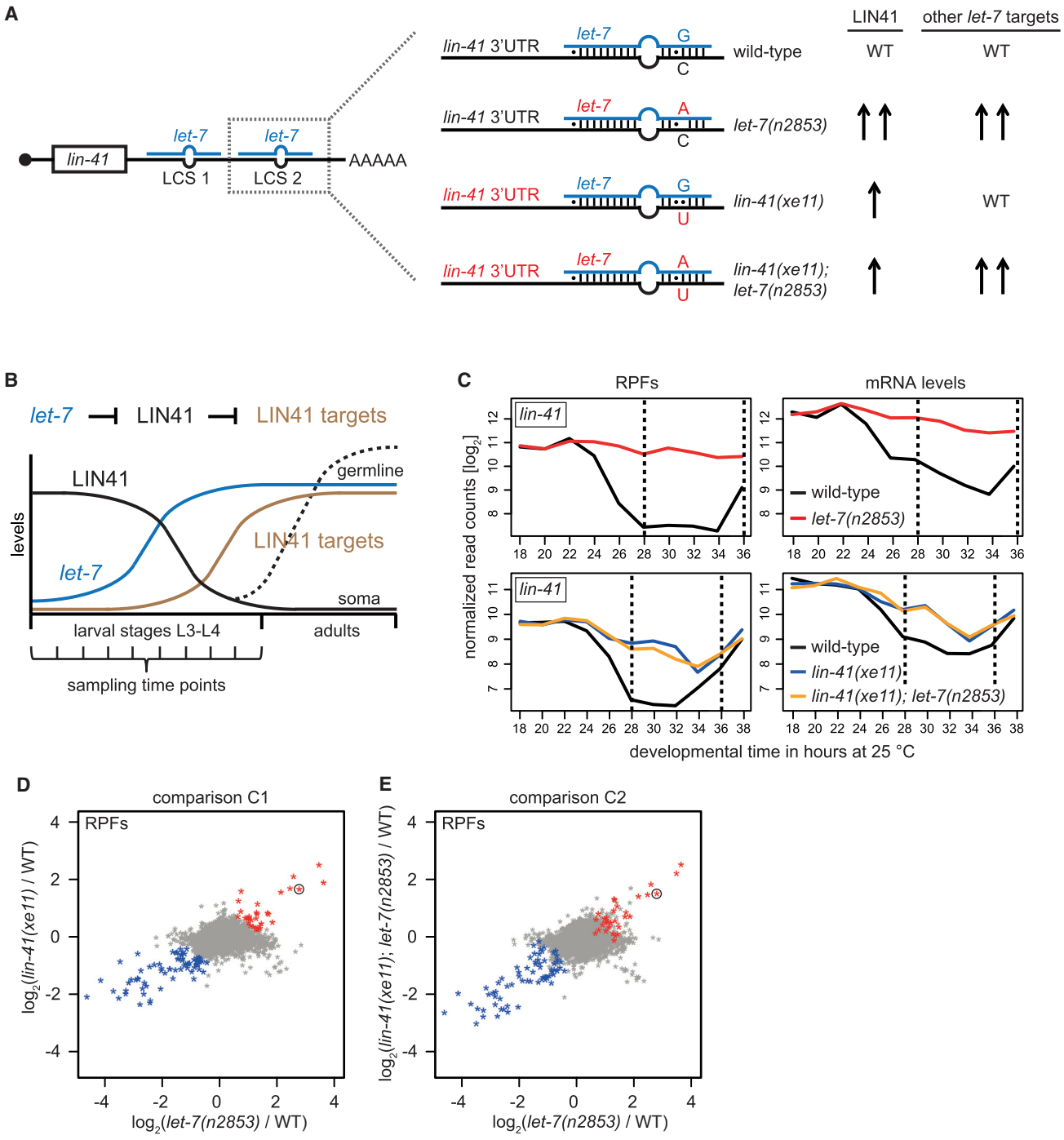

Figure 1. Gene Expression Changes Caused by Dysregulation of LIN41

(A) Schematic of *let-7* miRNA binding to the two functional *let-7* complementary sites (LCSs) in the *lin-41* 3′ UTR (Vella et al., 2004). Blow-ups illustrate the effects of mutations for only the second LCS. Lines indicate Watson-Crick base pairs, dots represent wobble base pairs, and mutated genes and nucleotides are in red. Columns on the right illustrate how the levels of LIN41 and of other *let-7* targets are affected (WT, wild-type levels; one arrow, partial de-silencing; two arrows, full de-silencing).

(B) Schematic of developmental expression patterns of LIN41, its regulator *let-7*, and its hypothetical targets. Following silencing of LIN41 in the soma by *let-7*, LIN41 accumulates massively in adult germlines. Synchronized worm populations were harvested bi-hourly as indicated.

(C) *lin-41* expression over time at the level of ribosome-protected fragments (RPFs, left) and mRNA (right). Upper and lower panels represent two independent experiments. Fewer reads obtained from the second time course experiment account for generally lower normalized $\log_2$ read counts relative to the first time course experiment. The two dashed lines indicate the window of time points pooled for differential gene expression analysis in (D) and (E).

(legend continued on next page)

2000), to LIN41 functions in the adult germline and larval epidermis, respectively. However, both await experimental validation as direct LIN41 targets.

Here we identify direct targets of *C. elegans* LIN41. These include *lin-29A/EGR* and *mab-10/NAB*, implicated in LIN41-dependent mammalian cell fate reprogramming (Worringer et al., 2014), implying evolutionary conservation of a LIN41-dependent fundamental stem cell fate regulatory process. We find that LIN41 can silence mRNAs through two distinct mechanisms, repression of translation or destabilization. Unexpectedly, the choice of mechanism depends on the target and is instructed by where on the mRNA LIN41 binds: binding to the 5′ UTR elicits translational repression, and binding to the 3′ UTR elicits transcript degradation. We are currently aware of two additional examples of animal RBPs with position-dependent dual activities (Beckmann et al., 2005; Kühn, 2015), each with unique combinations of activities. Therefore, more such RBPs may remain to be discovered.

RESULTS

Dysregulation of LIN41 Quantitatively Explains Gene Expression Changes in *let-7* Mutant Animals

To elucidate the regulatory functions of LIN41, we compared changes in gene expression between wild-type animals and previously described *C. elegans* mutants, in which LIN41 is uncoupled from repression by *let-7* to different extents as follows (Figure 1A): (1) *let-7*(*n2853*) mutant animals carry a point mutation in the *let-7* seed sequence (Reinhart et al., 2000) that prevents *let-7* activity at 25°C, resulting in complete de-silencing of *lin-41* and the other *let-7* targets. Thus, a comparison to wild-type animals identifies any gene dysregulated in the absence of *let-7*, be it by direct *let-7* targeting or as a secondary effect. (2) *lin-41*(*xe11*) mutant animals contain two point mutations in the *lin-41* 3′ UTR, one in each of the two functional *let-7* complementary sites (LCSs) (Ecsedi et al., 2015). The resulting replacement of a G:C Watson-Crick base pair by a G:U wobble pair in the two seed:seed-match hybrids formed with wild-type *let-7* causes partial but specific de-silencing of *lin-41*. (3) *lin-41*(*xe11*); *let-7*(*n2853*) double-mutant animals carry the point mutations of both (1) and (2). Hence, the mutation in the let-7 seed sequence disrupts silencing of all *let-7* targets but *lin-41*, whose two LCSs each contain a compensatory mutation in the seed match that restores base pairing. However, *let-7* levels in the *let-7*(*n2853*) genetic background are reduced (Chatterjee and Großhans, 2009; Reinhart et al., 2000), preventing a full, wild-type-like repression of *lin-41* in this situation. Thus, *lin-41*(*xe11*); *let-7*(*n2853*) double-mutant animals exhibit a similar partial de-silencing of *lin-41* as the *lin-41*(*xe11*) single-mutant animals (see below and Ecsedi et al., 2015), but full de-silencing of all other *let-7* targets.

To identify transcripts that LIN41 might regulate through translational repression or degradation, we performed ribosome profiling and RNA sequencing (RNA-seq) on synchronized worm populations, sampled every 2 hr during development from late larval stage 2 (L2)/early L3 to late L4/young adult stages (Figure 1B; Tables S1 and S2 provide normalized $\log_2$ read counts). These time course experiments offered two advantages over single time point measurements. First, because *let-7* levels increase greatly between L3 and L4 stages (Reinhart et al., 2000), *lin-41* is presumably increasingly repressed in this time window (Figure 1B). Since LIN41 was suggested to be an RBP with repressive function, we predicted LIN41 downregulation to cause an accumulation of its targets over time. Second, as gene expression in *C. elegans* is highly dynamic, with thousands of genes exhibiting rhythmic expression with high amplitude (Hendriks et al., 2014), single time point experiments may be prone to expression artifacts through differences in developmental rates (and thus misalignment of time points) and/or population synchrony between wild-type and mutant animals (Figure S1).

We compared wild-type to *let-7*(*n2853*) animals in a first experiment, and we compared a biological wild-type replicate to both *lin-41*(*xe11*) single- and *lin-41*(*xe11*); *let-7*(*n2853*) double-mutant animals in a second experiment. In wild-type worms, both *lin-41* mRNA and ribosome-protected fragment (RPF) levels started to decrease from late L3/early L4 stage on, corresponding to the time of increase in *let-7* expression (Figure 1C). They reached a plateau by early/mid-L4 before rising again in late L4 stage, when *lin-41* starts being expressed in the germline (Spike et al., 2014a; Tocchini et al., 2014) (data not shown). As observed previously (Bagga et al., 2005; Ding and Großhans, 2009), major decreases were apparent at the level of the transcript, but they appeared somewhat enhanced at the translational level. In *let-7*(*n2853*) mutant animals, both types of repression were completely eliminated, and *lin-41* mRNA and RPF levels remained at L3 level throughout L4. In *lin-41*(*xe11*) single- and *lin-41*(*xe11*); *let-7*(*n2853*) double-mutant animals, repression of *lin-41* occurred but was blunted relative to wild-type.

Next, we examined gene expression changes between the mutants and their corresponding wild-type controls, averaged from 28 to 36 hr of development, the time window of the *lin-41* repression plateau (Figure 1C). We focused on fold changes at the level of RPFs, as these would integrate RNA level and translational changes, and we performed two comparisons, referred to as "C1" and "C2." In C1, we examined the effect of fully dysregulating all *let-7* targets (in *let-7*(*n2853*) animals) versus partially dysregulating only LIN41 (in *lin-41*(*xe11*) animals) (Figure 1D). This revealed substantial similarity in the genes dysregulated in each mutant relative to wild-type. In agreement with higher levels of LIN41 in the *let-7*(*n2853*) than in the *lin-41*(*xe11*) mutant background, the extent of dysregulation of individual genes was consistently larger in the *let-7* mutant animals. Taking this into account, we identified sets of genes consistently up- or downregulated in the two mutants (Figure 1D, red and blue

(D and E) Scatterplots depicting mutant to wild-type $\log_2$ fold changes in normalized RPF read counts for each gene. Gene expression changes are compared between (D) *let-7*(*n2853*) and *lin-41*(*xe11*) and (E) *let-7*(*n2853*) and *lin-41*(*xe11*); *let-7*(*n2853*) mutant animals. In (D) and (E), genes upregulated in both *let-7*(*n2853*) and *lin-41*(*xe11*) mutants are colored red, those downregulated are colored blue (METHODS), and *lin-41* is circled. Each comparison (x axis versus y axis) is between two independent experiments, with independent wild-type replicates.
See also Figure S1 and Tables S1 and S2.

asterisks, respectively), i.e., genes changed upon LIN41 dysregulation.

The similarity of gene expression changes caused by the two distinct mutations in C1 suggested that LIN41 upregulation accounted for many of the gene expression changes in *let-7*(*n2853*) animals. To test this notion, we examined, in C2, the effect of fully dysregulating all *let-7* targets in a context of complete (in *let-7*(*n2853*) animals) or partial (in *lin-41*(*xe11*); *let-7*(*n2853*) double-mutant animals) LIN41 de-silencing (Figure 1E). As expected from the shared *let-7* mutation, gene expression changes overlapped extensively. Strikingly, however, when we highlighted the genes that were consistently up- or downregulated in C1, these were largely identical to those consistently dysregulated in C2. Only a few additional upregulated genes emerged that had not been upregulated in *lin-41*(*xe11*) in C1 (gray asterisks in upper right quadrant of Figure 1E). These included direct *let-7* targets such as *daf-12* (Großhans et al., 2005) and *hbl-1* (Abrahante et al., 2003) (Figures S2A and S2B). Hence, although the *let-7*(*n2853*) mutation de-silences *let-7* targets broadly, secondary changes largely depend on dysregulation of *lin-41*. Indeed, the magnitude of gene expression changes appeared proportionate to the extent of *lin-41* de-silencing, i.e., it was greater in *let-7*(*n2853*) than in *lin-41*(*xe11*) or *lin-41*(*xe11*); *let-7*(*n2853*) mutant animals. We conclude that *let-7* effects on gene expression are extensively and quantitatively explained by dysregulation of LIN41 as its primary target.

Identification of Direct LIN41 Target Genes

To identify direct targets of LIN41, we visually examined temporal changes in gene expression for the selected genes changed upon LIN41 dysregulation, reasoning that effects on the levels of primary targets should precede those on the levels of secondary targets. The first gene that consistently changed in the various mutants relative to wild-type animals was *lin-41*, whose expression was increased in all mutants relative to wild-type by 24 hr (Figures 1C and 2A; Table S3). For the six genes affected next, termed "mid" in Figure 2A, RPF levels were all decreased in the mutants relative to wild-type. Specifically, their levels all increased in L4-stage wild-type animals as LIN41 disappeared, but they remained low in L4-stage *let-7*(*n2853*) or *lin-41*(*xe11*) mutant animals, which retain high LIN41 levels (Figures 2B and S2C). This is the pattern we would predict for direct targets of LIN41, and the group included *lin-29*, a previously proposed target of LIN41 (Slack et al., 2000). Subsequently affected genes were either up- or downregulated, consistent with secondary effects dominating in this class. Closer inspection of the expression patterns of the mid genes revealed that, for five of the six genes, both transcript and RPF levels changed (Figures 2B and S2C), suggesting potential regulation at the level of transcript stability. *lin-29* was an exception, where little or no difference occurred on the mRNA level between wild-type and mutant animals, but major differences occurred on the RPF level (Figure 2B). This finding suggested a predominant or exclusive regulation of *lin-29* at the translational level.

To test if the six mid genes are directly regulated by LIN41, we sought to determine whether LIN41 physically interacted with their mRNAs in L3/L4-stage animals. By immunoprecipitation (IP) of a functional FLAG::GFP::LIN41 fusion protein, we detected binding of LIN41 to *lin-29* and *mab-10* mRNAs as well as, to a lesser extent, *mab-3* and *dmd-3* mRNAs (Figure 2C). In contrast, the other two candidate targets, *ceh-60* and *Y54G2A.3*, behaved similarly to the negative control mRNAs, *act-1* and *unc-54*. Binding of *lin-29*, *mab-10*, *mab-3*, and *dmd-3* mRNAs was specific in that it was not observed with IP of another RBP, FLAG::GFP::SART-3 (Rüegger et al., 2015) (Figure 2C). We conclude that these four genes may be direct targets of LIN41.

LIN41-Dependent Regulation through Target Gene 3′ UTRs

RBPs frequently confer regulation by binding to the 3′ UTRs of target mRNAs, and LIN41 is capable of repressing target reporter genes in this manner in mammalian cells in vitro (Chang et al., 2012; Loedige et al., 2013). To determine whether LIN41 exerts a similar function in vivo in *C. elegans*, we constructed reporter transgenes consisting of the ubiquitously and constitutively expressing *dpy-30* promoter, a sequence encoding GFP fused to a destabilizing PEST sequence and nuclear H2B to achieve greater expression dynamics and nuclear concentration of the signal, respectively, and a 3′ UTR of interest (Figure 3). All transgenes were integrated in single copy into the same genomic location, and expression was examined by confocal microscopy in the epidermis of L3-stage animals, i.e., prior to LIN41 repression by *let-7*. For each of the following GFP reporter experiments, the GFP signals for at least ten worms were observed to verify that they were comparable among different worms in each transgenic line and for each condition.

As a control, we utilized the *unc-54* 3′ UTR, not known to confer any post-transcriptional regulation. As expected, GFP signal was readily detectable in the epidermis for this reporter, irrespective of the presence of LIN41 (Figure 3). By contrast, a reporter containing the *mab-10* 3′ UTR was silenced extensively in the same tissue. Silencing was dependent on LIN41, as RNAi-mediated depletion of LIN41 relieved it. Use of the *mab-3* and *dmd-3* 3′ UTR yielded similar results. Surprisingly, however, we observed no significant repressive activity of LIN41 on the *lin-29* 3′ UTR. Taken together, these and the above findings establish *mab-3*, *mab-10*, and *dmd-3* as bona fide LIN41 targets, whose regulation involves transcript degradation conferred by their 3′ UTRs.

LIN41 Regulates Only the A Isoform of *lin-29*

To understand *lin-29* translational regulation, we inspected its RPF profiles in more detail. Inhibition of translation initiation would lead to a uniform decrease in RPF coverage along the *lin-29* open reading frame (ORF), while inhibition of translation elongation or premature ribosome drop-off could lead to a decrease in RPF coverage toward the 3′ end of the ORF. To look at changes in the RPF distribution in the *let-7* mutant compared to wild-type, we calculated the fold repression on a per-exon basis, summing up the five time points of the *lin-41* repression plateau (28–36 hr, see Figure 1C). As a control, we performed the same analysis for mRNA reads. Unexpectedly, we observed that the sustained *lin-41* expression in *let-7* mutant animals caused an apparently greater translational repression toward the *lin-29* 5′ end than the 3′ end, with an ~10-fold

A

change in time course	genes up	genes down
early	1*	0
mid	0	6**
late	24	64

*lin-41 **ceh-60
mab-10
lin-29
dmd-3
mab-3
Y54G2A.3

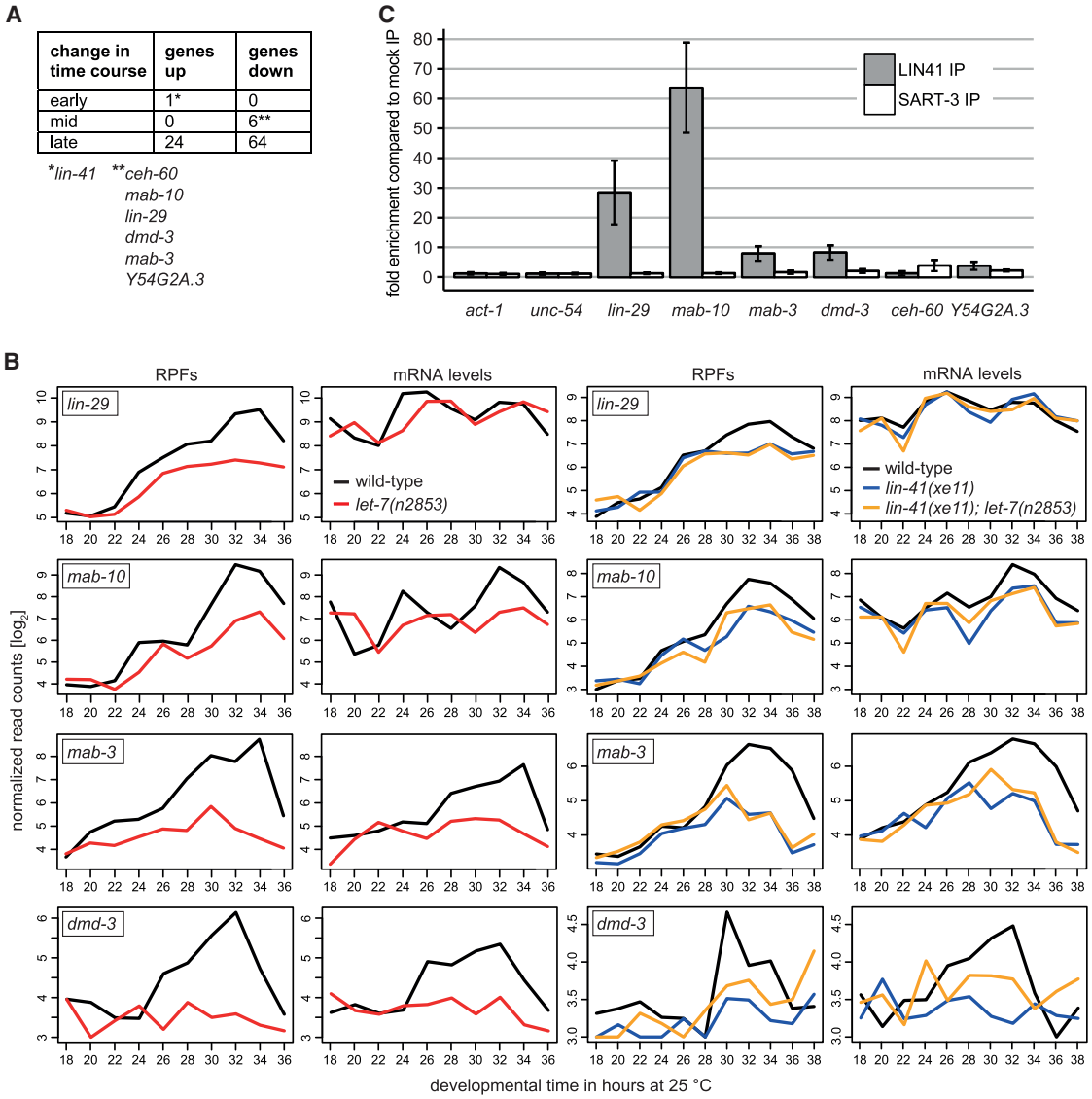

Figure 2. Identification of LIN41 Target mRNAs

(A) Genes differentially expressed in all examined mutant (*let-7*(*n2853*), *lin-41*(*xe11*), and *lin-41*(*xe11*); *let-7*(*n2853*)) relative to wild-type animals are listed according to the earliest time point of consistent dysregulation at the RPF level. "Up" and "down" refer to expression changes in mutants relative to wild-type, not to expression changes over time. Table S3 provides a complete list and details.

(B) Expression of candidate LIN41 target genes over development is shown.

(C) RT-qPCR analysis on RNA co-immunoprecipitated with FLAG::GFP::LIN41 or an unrelated RBP, FLAG::GFP::SART-3. mRNA levels of six candidate LIN41 targets and the negative controls *act-1* and *unc-54* were determined. Immunoprecipitation (IP) occurred through an anti-FLAG antibody, and fold enrichments were calculated relative to anti-FLAG IP in non-transgenic (wild-type) animals. Worms were harvested as semi-synchronous L3/L4-stage animals. n = 4 biological replicates, data as mean ± SEM.

See also Figure S2 and Table S3.

repression for each of the exons one through four but only an ~2-fold repression for each of the other exons (Figure 4A). In contrast to RPF levels, mRNA levels were unaffected for any exon.

We reasoned that, rather than pointing to a specific mechanism of translational repression, the difference between exons might reflect differential regulation of *lin-29* isoforms, as the two reported *lin-29* isoforms encompass exons 1–11 (long isoform *lin-29A*) and 5–11 (short isoform *lin-29B*), respectively (Figure 4A) (Rougvie and Ambros, 1995). A preferential regulation of *lin-29A* by LIN41 would explain why exons 1–4, which are exclusive to *lin-29A*, are more strongly regulated than exons 5–11, which are shared by the A and B isoforms. In other words, the change in RPF reads on exons 5–11 caused by regulation of *lin-29A* might be partially masked by reads from the unregulated *lin-29B* isoform. The difference between exons 1–4 and exons

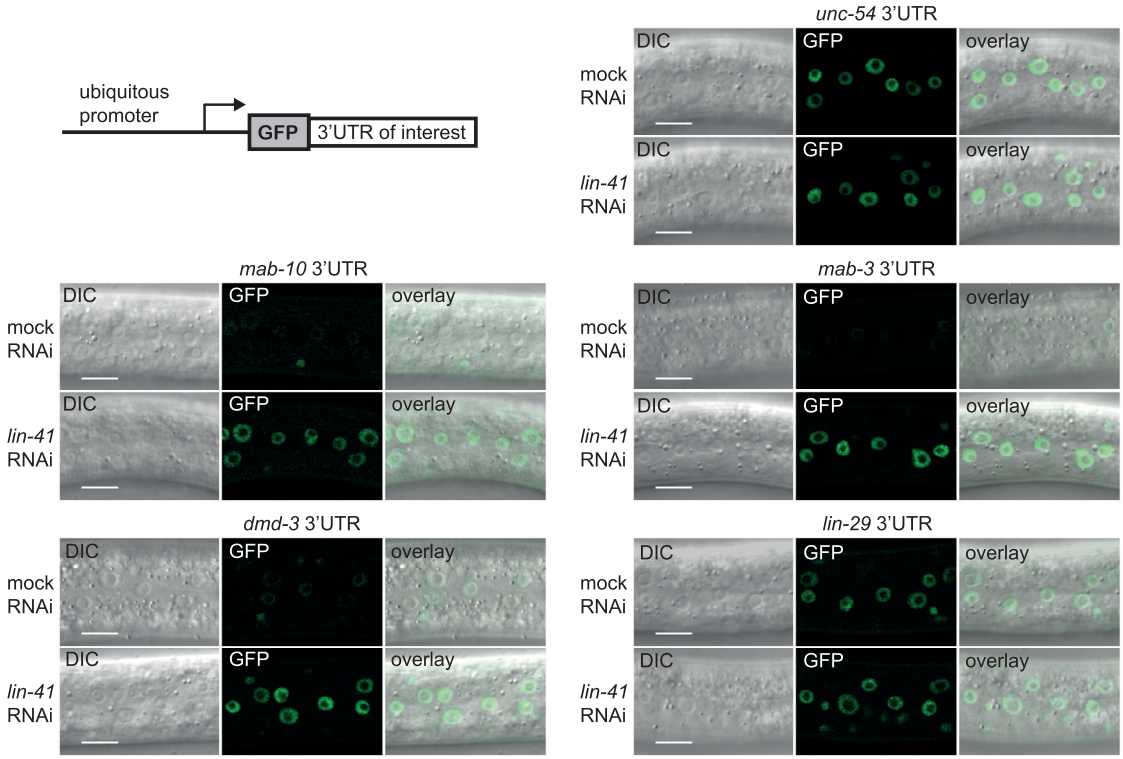

Figure 3. The 3′ UTRs of *mab-10*, *mab-3*, and *dmd-3* mRNAs Confer LIN41-Dependent Gene Silencing

The constitutive *dpy-30* promoter drives ubiquitous expression of mRNA encoding a nuclear-localized fluorophore (GFP(PEST)::H2B; labeled "GFP") and containing to the 3′ UTRs of candidate LIN41 targets or of *unc-54* as a control. Animals were grown on *lin-41* RNAi or mock RNAi bacteria, and images of epidermal nuclei of live early L3-stage worms were acquired by confocal imaging. Shown are images with differential interference contrast (DIC), GFP (identical settings for both RNAi conditions), and the overlay of the two. Scale bars here and in all other figures, 10 μm.

5–11 also held true when examining the effect on *lin-29* translation over time (Figure 4B) and when performing the same analyses with the *lin-41*(*xe11*) and *lin-41*(*xe11*); *let-7*(*n2853*) mutant animals (Figures S3A and S3B). To verify preferential regulation of *lin-29A* by LIN41, we examined the extent to which isoforms co-immunoprecipitated with LIN41. Consistent with preferential binding to *lin-29A*, LIN41 IP enriched this mRNA isoform, but not the shorter *lin-29B* isoform (Figures 4C and S3C).

To confirm the differential effect of LIN41 on LIN-29 isoforms directly on the protein level, we used genome editing to place a GFP::3xFLAG tag on the shared C terminus of endogenous LIN-29A and LIN-29B. These animals appear overtly wild-type, indicating functionality of the tagged protein, and they recapitulate temporal and spatial expression patterns previously established by immunofluorescence (Bettinger et al., 1996, 1997; data not shown). Moreover, and consistent with LIN41-mediated silencing, LIN-29::GFP protein was undetectable in the epidermis of live L3-stage animals exposed to mock RNAi, but it revealed strong nuclear accumulation upon LIN41 depletion (Figure 4D). By contrast, L3-stage nuclear accumulation of LIN-29 occurred in some non-epidermal tissues, such as the pharynx, independently of LIN41 depletion.

To test for differential regulation of the two LIN-29 protein isoforms, we performed western blotting. This revealed that, in L3-stage animals and thus in the presence of LIN41, LIN-29B, but not LIN-29A, was detectable in total animal lysates (Figures 4E and S3D). Moreover, little or no change occurred for LIN-29B when animals were depleted of LIN41. In striking contrast, LIN41 depletion caused a strong accumulation of LIN-29A protein. We conclude that LIN41 preferentially or exclusively regulates isoform A of LIN-29. As depletion of LIN41 left *lin-29A* mRNA levels unaffected (Figures 4F, S3E, and S3F), this regulation occurred on the level of translation, as expected from the ribosome profiling experiment.

Silencing of *lin-29A* Occurs through Its 5′ UTR

Although the *lin-29* 3′ UTR had no repressive activity (Figure 3), we were able to recapitulate the strong endogenous *lin-29A* regulation with a reporter construct, when we placed GFP(PEST)::H2B between the 4-kb region upstream of the *lin-29A* start codon and the *lin-29A* 3′ UTR (Figure 5A). The 4-kb region contained both the putative *lin-29A* promoter and 5′ UTR, but regulation appeared unlikely to involve the promoter since modulation of LIN41 left endogenous *lin-29A* mRNA levels unaffected. Therefore, we examined the consequences of replacing the first exon of the *lin-29A* 5′ UTR with an *act-1* 5′ UTR exon. This caused a loss of repression, in contrast to exchange of the *lin-29* 3′ UTR by the *unc-54* 3′ UTR (Figure 5A). Hence, LIN41-dependent silencing requires an intact *lin-29A* 5′ UTR.

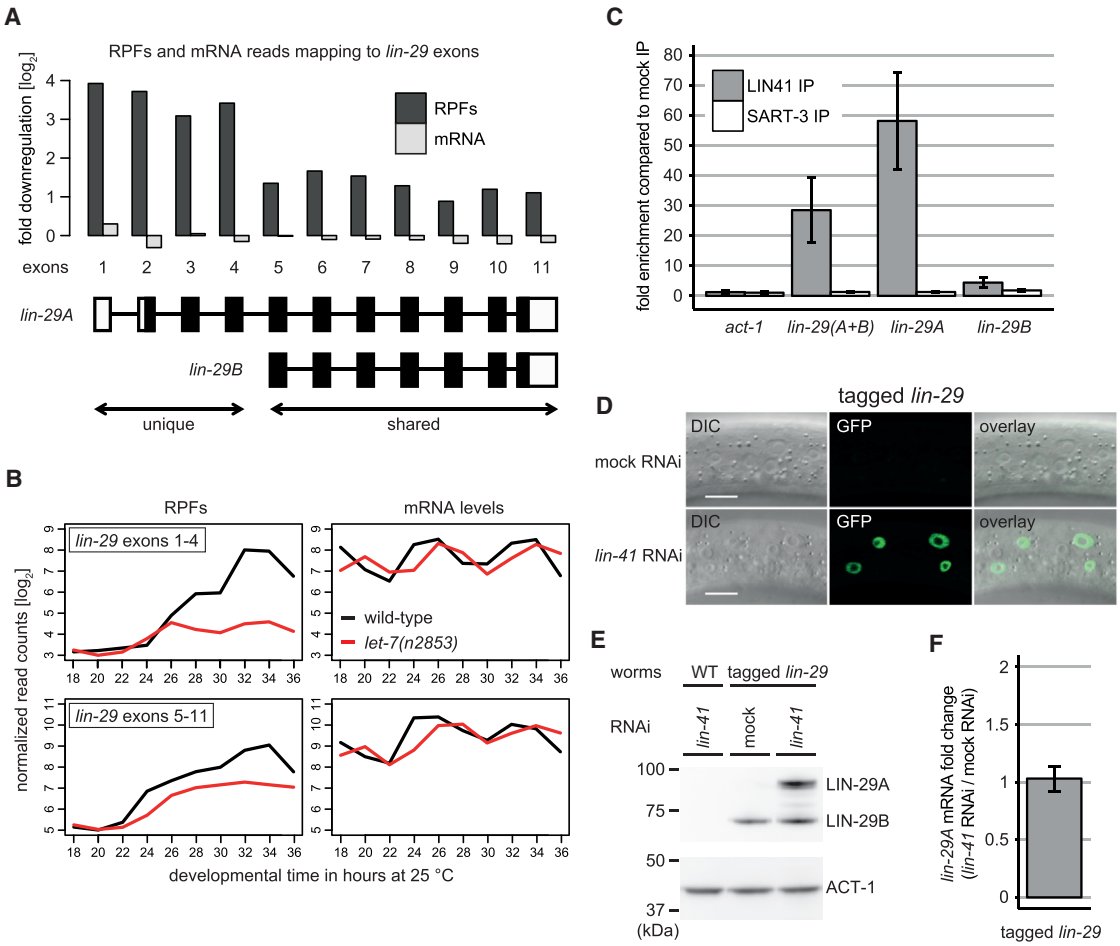

Figure 4. LIN41 Inhibits the Translation of Only One of the Two *lin-29* Isoforms

(A) Quantification of the fold downregulation in RPF and mRNA reads (log_2) in *let-7* mutant relative to wild-type worms for each exon of the *lin-29* gene. Reads were pooled from the five time points used for differential gene expression analysis in Figures 1D and 1E (28–36 hr). Below the histogram, a schematic representation (not to scale) depicts *lin-29* isoforms (open boxes, UTRs; filled boxes, coding sequence).

(B) Expression of *lin-29* over development, separated by reads pooled from exons 1–4 (unique to *lin-29A*) and exons 5–11 (shared between *lin-29A* and *lin-29B*), is shown.

(C) RT-qPCR analysis to test for enrichment of the two *lin-29* isoform mRNAs by LIN41 coIP, as described for Figure 2C. *act-1* mRNA is a negative control. The unique SL1 splice leader sites were exploited to distinguish between the two *lin-29* isoforms (see Figure S3C). n = 4 biological replicates, data as mean ± SEM.

(D) Confocal images show the endogenously tagged LIN-29 protein, accumulating in epidermal nuclei of early L3-stage *lin-29*(*xe61*[*lin-29*::*gfp*::*3xflag*]) worms upon depletion of LIN41.

(E) Western blot analysis to detect endogenous GFP::3xFLAG-tagged LIN-29A and LIN-29B proteins in early L3-stage *lin-29*(*xe61*[*lin-29*::*gfp*::*3xflag*]) animals using an anti-FLAG antibody. ACT-1 was detected as a loading control. Wild-type (WT) worms without the inserted GFP::3xFLAG tag control for antibody specificity.

(F) RT-qPCR analysis to measure the fold change of *lin-29A* mRNA levels (normalized by *act-1* mRNA levels) in early L3-stage *lin-29*(*xe61*[*lin-29*::*gfp*::*3xflag*]) animals exposed to *lin-41* RNAi relative to mock RNAi is shown. n = 3 biological replicates, data as mean ± SEM.

See also Figure S3.

To test whether the *lin-29A* 5′ UTR was sufficient for LIN41-mediated silencing, we placed it upstream of GFP and the *unc-54* 3′ UTR in a reporter expressed from the constitutively active *dpy-30* promoter. The *lin-29A* 5′ UTR comprises exon 1 and part of exon 2. Therefore, we generated two reporters that either included the 5′ UTR sequences from both exons and the intron or only exon 1. Both reporters were silenced by LIN41 (Figure 5B). By contrast, constructs that contained either the complete sequence or only exon 1 of the *mab-10* 5′ UTR were not detectably regulated (Figures 5B and S4A). We conclude that exon 1 of the 5′ UTR is both necessary and sufficient for *lin-29A* silencing through LIN41 and that repression is independent of 5′ UTR splicing.

LIN41 Can Bind Directly to Its Target mRNAs

The NHL domain of the TRIM-NHL proteins Brat and LIN41 can bind to RNA (Kwon et al., 2013; Loedige et al., 2014, 2015). To test whether LIN41 may contact its mRNA targets directly via its NHL domain, we expressed a recombinant LIN41 variant consisting of the C-terminal Filamin and NHL domains

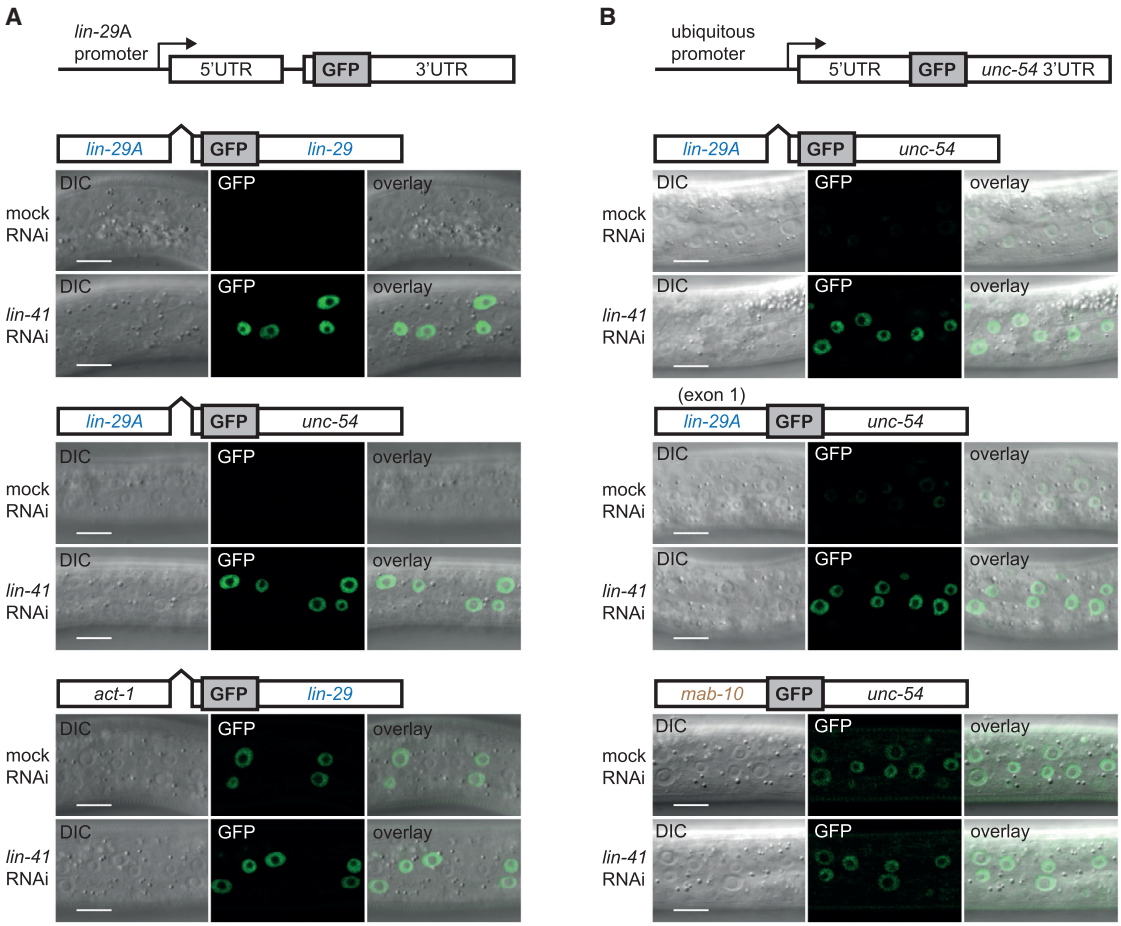

Figure 5. The 5′ UTR of *lin-29A* Mediates LIN41-Dependent Translational Repression

(A and B) Micrographs show early L3-stage animals, exposed to *lin-41* or mock RNAi, expressing nuclear-localized GFP reporters with the indicated 5′ and 3′ UTRs from (A) the *lin-29A* promoter or (B) the *dpy-30* promoter. See also Figure S4.

(Figure S5A). Using electrophoretic mobility shift assays (EMSAs), we found that the 194-nt-long 5′ UTR segment of *lin-29A* exon 1 was bound by recombinant LIN41, whereas a control fragment of the *unc-54* 3′ UTR was not (Figure 6A). Binding to the *lin-29A* 5′ UTR appears to involve multiple binding sites, since LIN41 bound to three different and partially overlapping ~100-nt fragments of it (Figures S5B and S5E). However, affinity of each fragment was reduced relative to the full-length fragment (Figure S5F), and, accordingly, none of the ~100-nt fragments sufficed for LIN41-mediated repression in vivo (Figure S6A).

We used six consecutive 200-nt fragments, overlapping by 50 nt, to test binding of LIN41 to the *mab-10* 3′ UTR. Whereas LIN41 failed to bind the first and the last two segments, it did bind each of three partially overlapping segments in the middle of the 3′ UTR (Figures 6B and 6C). As expected, the *mab-10* 5′ UTR was not bound by LIN41. The two non-overlapping *mab-10* 3′ UTR segments with clear EMSA shifts, parts 2 and 4, individually sufficed for repression of a GFP reporter when transplanted into the *unc-54* 3′ UTR (Figure 6D), confirming that there are at least two LIN41-binding sites on the *mab-10* 3′ UTR. When trying to delineate the minimal region needed for LIN41 binding to *mab-10* 3′ UTR parts 2 and 4, we found that LIN41 bound shorter ~100-nt RNA stretches poorly if at all (Figures S5C–S5E), similar to what we found with the *lin-29A* 5′ UTR. In conclusion, LIN41 has direct RNA-binding activity whose specificity in vitro reflects its target silencing specificity in vivo.

LIN41 Activity on *lin-29A* Differs from that on the Other Targets

To examine the silencing mechanism acting on reporter genes, we measured whole-worm *gfp* transcript levels for *lin-29A* promoter-containing constructs in early L3-stage worm lysates. As for endogenous *lin-29A* (Figure 4F), *lin-41*(*RNAi*) did not affect transcript levels of the reporter containing both *lin-29A* 5′ UTR and 3′ UTR (Figures 7A and S4C). We can exclude that this is due to use of whole-animal lysates, as they permit ready detection of LIN-29A repression by western blot (Figures 4E and S3D). Indeed, in early L3 stage, the reporter is silenced by LIN41 broadly across the epidermis, revealing LIN41 refractory expression in only a single cell, the anchor cell (data not shown). Hence, the absence

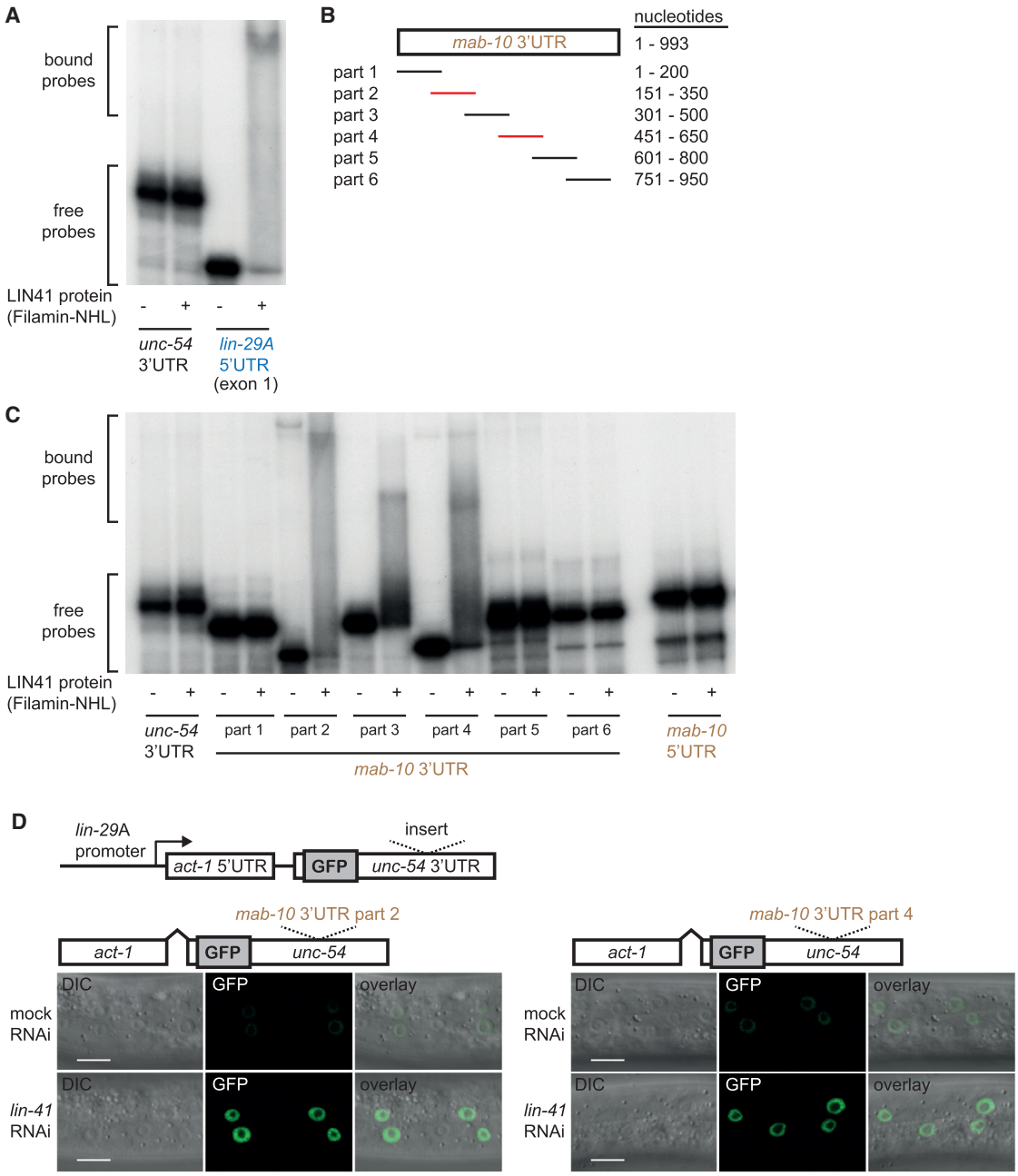

Figure 6. LIN41 Directly Binds to Its Target mRNAs

(A) Autoradiograph showing binding of LIN41 to the *lin-29A* 5′ UTR (194 nt). A 198-nt fragment from the *unc-54* 3′ UTR is used as a negative control.

(B) Schematic showing overlapping 200-nt-long radioactively labeled RNA gel-shift probes spanning the *mab-10* 3′ UTR, with those binding most efficiently to LIN41 in red.

(C) Autoradiograph showing binding of LIN41 to three 200-nt fragments (parts 2–4) from the *mab-10* 3′ UTR, but not to other *mab-10* 3′ UTR parts, the *mab-10* 5′ UTR (244 nt), or the control *unc-54* 3′ UTR fragment.

(D) Micrographs of early L3-stage animals, exposed to *lin-41* or mock RNAi, expressing nuclear-localized GFP reporters from the *lin-29A* promoter. The reporters contain the unregulated *act-1* 5′ UTR exon and the *unc-54* 3′ UTR, with either *mab-10* 3′ UTR part 2 or 4 as an insert.

For (A) and (C), the LIN41 protein used in the assays is N-terminally truncated and contains the Filamin and NHL domains.

See also Figures S5 and S6.

of detectable transcript degradation shows that the reporter recapitulates regulation of endogenous *lin-29A* through translational repression.

We envisioned three scenarios by which the *lin-29A* transcript might escape degradation by LIN41. First, LIN41 activity on this target might differ from that on other targets. Second, the *lin-29A*

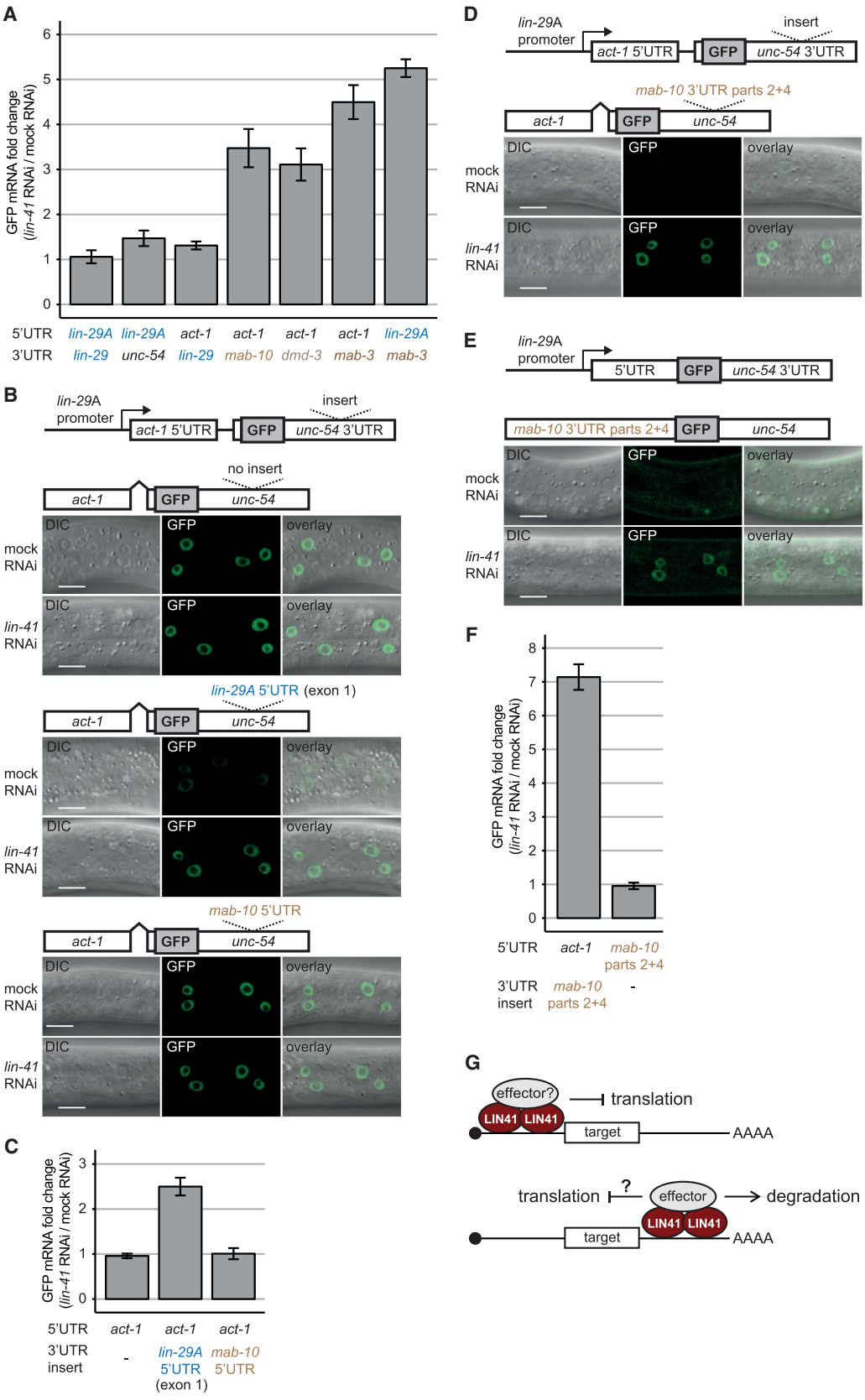

(legend on next page)

3′ UTR and/or 5′ UTR might specifically protect the transcript from decay. Third, the epidermis as a major organ of *lin-29A* expression might lack the capacity to execute LIN41-mediated degradation altogether. To distinguish among these possibilities, we quantified transcript level changes for additional reporters (summarized in Figure S4F). First, we compared the reporter transgenes containing the *lin-29A* 5′ UTR and either the *lin-29* 3′ UTR or the *unc-54* 3′ UTR, both silenced at the GFP level (Figure 5A). Neither reporter revealed substantial LIN41-dependent changes in mRNA levels (Figure 7A), excluding a general stabilizing effect of the *lin-29* 3′ UTR. Next, we examined transcript levels of the reporter transgenes that shared the *lin-29A* promoter and *act-1* 5′ UTR but contained the 3′ UTRs of *lin-29*, *mab-10*, *dmd-3*, or *mab-3*, respectively (Figures 7A and S4B). Major LIN41-dependent decreases in transcript levels occurred with the latter three, excluding a lack of degradative activity in the epidermis. Finally, we tested a construct that contained the *lin-29A* 5′ UTR and the *mab-3* 3′ UTR, and we observed transcript degradation (Figures 7A and S4B). Thus, degradation prevailed over translational repression and the *lin-29A* 5′ UTR could not inhibit mRNA degradation. In summary, because there is LIN41-induced degradative activity in the epidermis and the reporters with *lin-29A* 5′ UTR or 3′ UTR are not inherently resistant to degradation, we conclude that, on *lin-29A*, the mode of repression by LIN41 truly differs from that on the other target genes.

Relocation of LIN41-Binding Sites Alters the Mode of Silencing

Given that *lin-29A* repression differed in both the location of the repressive element and the mechanism of action, we wondered if the former instructed the latter. Therefore, we examined if and how a reporter was repressed when the LIN41-binding site of the *lin-29A* 5′ UTR was placed in a 3′ UTR context. When transplanting the *lin-29A* 5′ UTR exon 1 into the *unc-54* 3′ UTR, we found that GFP expression from the resulting reporter transcript was indeed repressed (Figure 7B). Although the extent of repression seemed less than what was seen when the same element was present in the 5′ UTR, silencing was specific in that it depended on LIN41 and the inserted sequence. Strikingly, when examining the transcript levels of the reporter, we observed a substantial reduction in the presence of LIN41 (Figures 7C and S4D). Therefore, the same element that caused translational repression when present in a 5′ UTR specifically induced transcript degradation when occurring in a 3′ UTR.

To test if, conversely, transplantation of a 3′ UTR-binding site into a 5′ UTR sufficed to switch the mechanism of LIN41-mediated silencing from degradation to translational repression, we focused on the *mab-10* 3′ UTR. Although parts 2 and 4 each bound to LIN41 in vitro and, within a 3′ UTR, conferred reporter repression in vivo (Figures 6C and 6D), they were non-functional when individually used as a 5′ UTR, causing either no regulation or a general loss of translation (Figure S6B). However, when we combined them into a single fragment, the two parts sufficed for LIN41-dependent GFP repression, not only when placed in the heterologous *unc-54* 3′ UTR (Figure 7D) but also when utilized as a 5′ UTR (Figure 7E). In the ectopic 5′ UTR context, repression no longer relied on reporter gene degradation, indicating a switch to translational repression (Figures 7F and S4E). Hence, the two transplantation experiments demonstrate that the location of the LIN41-repressive element is a major determinant of the LIN41 mechanism of action (Figure 7G).

DISCUSSION

Previous work from in vitro cell culture revealed that LIN41 utilizes transcript degradation as a mechanism of action (Chang et al., 2012; Loedige et al., 2013; Mitschka et al., 2015). Here we confirm such activity for *mab-10*, *mab-3*, and *dmd-3* in vivo, but additionally we demonstrate a second and distinct activity, namely, translational repression. Other RBPs, most prominently the miRNA-guided Argonaute proteins, are capable of silencing target transcripts through translational repression and degradation (Jonas and Izaurralde, 2015). However, translational repression typically augments rather than replaces transcript degradation as a silencing mechanism (Jonas and Izaurralde, 2015), and target determinants that favor one mechanism over the other have remained elusive. By contrast, we find that LIN41 can silence a target purely by translational repression. Moreover, we identify the location of LIN41-binding sites on its targets as a key determinant for the choice between translational inhibition and mRNA degradation.

The position-dependent function of LIN41 was unexpected, but we propose that a systematic evaluation of RBP activities might reveal location-dependent choice of activity as a more common, presently underappreciated feature of RBPs. Indeed, although further instances of RBPs that execute translational repression and RNA degradation in a position-dependent manner remain to be uncovered, metazoan iron regulatory proteins (IRPs) and *Drosophila melanogaster* sex-lethal (SXL) are two additional examples of position-dependent RBP functions: IRPs inhibit translation initiation when binding to a 5′ UTR, but they protect mRNA from degradation when binding to a 3′ UTR (Kühn, 2015), and SXL utilizes two distinct mechanisms to repress translation of the *male-specific lethal* (*msl*)*-2* mRNA through its 5′ UTR and 3′ UTR, respectively (Beckmann et al., 2005).

Figure 7. The Binding Location of LIN41 Determines Its Mode of Repression

(A, C, and F) RT-qPCR analysis of *lin-29A* promoter-driven GFP reporter mRNA levels. Depicted are the fold changes of GFP mRNA levels (normalized by *act-1* mRNA levels) from early L3-stage worms grown on *lin-41* RNAi relative to those grown on mock RNAi bacteria. n = 3 biological replicates, data as mean ± SEM.

(B, D, and E) Micrographs of early L3-stage animals, exposed to *lin-41* or mock RNAi, expressing nuclear-localized GFP reporters from the *lin-29A* promoter. (B) The reporters contain the unregulated *act-1* 5′ UTR exon and the *unc-54* 3′ UTR, without insert or with either the *lin-29A* 5′ UTR exon or the *mab-10* 5′ UTR as an insert. (D and E) The reporters contain a 400-nt-long fragment with fused *mab-10* 3′ UTR parts 2 and 4, either (D) as an insert within the *unc-54* 3′ UTR or (E) as a 5′ UTR.

(G) Position-dependent modes of action are applied by LIN41 to repress its mRNA targets (see the Discussion for details).

See also Figures S6 and S7.

It seems likely that LIN41, like other RBPs, triggers mRNA degradation through recruitment of dedicated effector proteins, i.e., deadenylases and/or ribonucleases (Figure 7G). These may then be absent when LIN41 binds to 5′ UTRs, or additional modulators or steric constraints may prevent their activity. Translational silencing also may involve recruitment of a dedicated machinery. If present also when LIN41 binds targets at their 3′ UTRs, LIN41 may always impose a translational block, although we observe little or no robust translational repression of such targets (Figures S7A–S7C). In analogy to certain models of miRNA activity (Jonas and Izaurralde, 2015), however, translational repression might then be tightly coupled to degradation, making degradation the observable net outcome. Alternatively, translational repression may depend on context features that restrict it to the 5′ UTR. For instance, LIN41 on the 5′ UTR may operate according to a roadblock model, whereby its binding, alone or in a complex, impedes ribosomal recruitment or scanning.

Irrespective of the scenario that applies, our data provide insight into the mechanism of translational repression. The fact that LIN41 binding reduces RPF levels homogenously along the length of the *lin-29A* transcript (within exons 1–4 and 5–11, Figures 4A and S3A) argues against both a block in elongation and premature ribosome drop-off as possible mechanisms, and instead it implies regulation at the level of translation initiation. Increased translation of upstream open reading frames (uORFs), preventing (re-)initiation on the main ORF, is a well-established means of repressing translation initiation in a 5′ UTR-dependent manner (Hinnebusch, 2005; Medenbach et al., 2011). However, we do not expect uORFs to contribute to silencing of *lin-29A*. The *lin-29A* 5′ UTR lacks cognate AUG start codons, and no RPFs accumulate from this 5′ UTR when *lin-29A* translation is repressed (Figures S7D and S7E). (Although we note that, for reasons that remain to be established, RPFs do accumulate from this region when LIN41 is absent.) In addition, whereas repressive activities of uORFs are dependent on position relative to the main ORF AUG start codon, we found that insertion of 65 extra nucleotides from the *act-1* 5′ UTR into two different positions of the *lin-29A* 5′ UTR did not detectably perturb repression (Figure S6C). Finally, the in vitro mapping (Figures 6A–6C and S5) and in vivo reporter (Figures 6D, 7D, and S6A) experiments suggest that both target 3′ and 5′ UTRs contain multiple LIN41-binding sites distributed over >100 nt that are required for effective binding and efficient silencing.

The four in vivo targets that we have uncovered and validated, *mab-3*, *dmd-3*, *mab-10*, and *lin-29A*, are likely to be major physiological effectors of LIN41. All four are known heterochronic (temporal patterning) genes, as are *let-7* and *lin-41* (Rougvie and Moss, 2013), and *lin-41* interacts genetically with *lin-29* and *mab-10* in controlling skin development (Harris and Horvitz, 2011; Reinhart et al., 2000; Slack et al., 2000) and with *dmd-3* in male tail development (Mason et al., 2008). The data that we present here supply missing mechanistic links of the heterochronic pathway by demonstrating that all four genes are direct LIN41 targets and by revealing that LIN41 regulates only one *lin-29* isoform, *lin-29A*.

LIN-29A and MAB-10 are particularly interesting LIN41 targets: LIN-29A is an early growth response (EGR)-type transcription factor of the Krüppel family, whereas MAB-10, orthologous to mammalian NAB1/2 (NGFI-A-binding proteins 1 and 2), is its transcription cofactor (Harris and Horvitz, 2011). Like LIN41, EGR and NAB proteins regulate proliferation and/or terminal differentiation programs in various animals and cell types, as exemplified previously (Du et al., 2014; Laslo et al., 2006; Le et al., 2005; Min et al., 2008; Nguyen et al., 1993; Topilko et al., 1994). Most strikingly, *let-7*, LIN41, and EGR1 were all shown to affect reprogramming efficiency of mammalian epidermal fibroblasts into induced pluripotent stem cells in vitro (Worringer et al., 2014). Although a mechanism of LIN41-mediated repression of EGR1 has not been established, EGR1 mRNA co-immunoprecipitates with LIN41 from human embryonic stem cells (Worringer et al., 2014). Hence, LIN41 may regulate stem cell fates through an evolutionarily conserved effector pair, LIN-29A/EGR and MAB-10/NAB.

STAR★METHODS

Detailed methods are provided in the online version of this paper and include the following:

- KEY RESOURCES TABLE
- CONTACT FOR REAGENT AND RESOURCE SHARING
- EXPERIMENTAL MODEL AND SUBJECT DETAILS
  - C. elegans
- METHOD DETAILS
  - Ribosome Profiling and Total RNA Sequencing
  - Construction of GFP Reporters
  - Confocal Imaging and RNA Extraction
  - RNA Co-immunoprecipitation (RIP)
  - RT-qPCR
  - Western Blotting
  - Tagging of Endogenous *lin-29* by CRISPR-Cas9
  - Electrophoretic Mobility Shift Assay
- QUANTIFICATION AND STATISTICAL ANALYSES
  - Ribosome Profiling and RNA-Seq Data Analysis
  - RT-qPCR Analysis
- DATA AND SOFTWARE AVAILABILITY

SUPPLEMENTAL INFORMATION

Supplemental Information includes seven figures and seven tables and can be found with this article online at http://dx.doi.org/10.1016/j.molcel.2016.12.010.

AUTHOR CONTRIBUTIONS

F.A. conceived the project; designed, performed, and computationally analyzed ribosome profiling and RNA-seq experiments; designed, performed, and analyzed confocal microscopy, RT-qPCR, and western blot experiments; created transgenic worm lines; and wrote the manuscript. P.K. purified the recombinant LIN41 protein fragment and performed and analyzed in vitro-binding experiments. H.B. performed RNA-IP experiments and created some transgenic worm lines. D.G. performed computational analysis of ribosome profiling and RNA-seq time courses. L.X. helped with cloning and worm injections. R.C. designed experiments. H.G. conceived the project, designed and analyzed experiments, and wrote the manuscript.

ACKNOWLEDGMENTS

We thank Monika Fasler and Magdalene Rausch for their help and support for this project. We are thankful to Iskra Katic for worm injections and comments on the manuscript, Jeremy Keusch for help in protein purification, and Giovanna Brancati for a reagent. We are grateful to Marc Buehler, Joerg Betschinger, Takashi Miki, Sarah Carl, Jun Liu, and Manuel de la Mata for discussions and comments on the manuscript. We thank Kirsten Jacobeit, Sophie Dessus-Babus, Stéphane Thiry, and Tim Roloff for help with library preparation and high-throughput sequencing and Laurent Gelman for help with confocal imaging. The work was partly supported by the Swiss National Science Foundation through grants 31003A_149402 (to R.C.), and grant 31003A_163447 and the NCCR RNA & Disease (to H.G.). Further funding for the research leading to these results was from the European Union Seventh Framework Programme (FP7/2007-2013) under grant agreement 241985 (European Research Council "miRTurn") and the Novartis Research Foundation through the FMI (to H.G.). P.K. has received funding for the research leading to these results from an EMBO Fellowship (ALTF 95-2015) that was co-funded by the European Commission support for Marie Curie Actions (LTFCOFUND2013, GA-2013-609409) and FMI. Some strains were provided by the Caenorhabditis Genetics Center (CGC), which is funded by the NIH Office of Research Infrastructure Programs (P40 OD010440).

Received: July 26, 2016
Revised: November 11, 2016
Accepted: December 13, 2016
Published: January 19, 2017

SUPPORTING CITATIONS

The following references appear in the Supplemental Information: Wright et al. (2011); Merritt et al. (2008).

REFERENCES

Abrahante, J.E., Daul, A.L., Li, M., Volk, M.L., Tennessen, J.M., Miller, E.A., and Rougvie, A.E. (2003). The Caenorhabditis elegans hunchback-like gene lin-57/hbl-1 controls developmental time and is regulated by microRNAs. Dev. Cell *4*, 625–637.

Aeschimann, F., Xiong, J., Arnold, A., Dieterich, C., and Großhans, H. (2015). Transcriptome-wide measurement of ribosomal occupancy by ribosome profiling. Methods *85*, 75–89.

Ahringer, J. (2006). Reverse genetics. WormBook, 1–43.

Ambros, V., and Horvitz, H.R. (1984). Heterochronic mutants of the nematode Caenorhabditis elegans. Science *226*, 409–416.

Bagga, S., Bracht, J., Hunter, S., Massirer, K., Holtz, J., Eachus, R., and Pasquinelli, A.E. (2005). Regulation by let-7 and lin-4 miRNAs results in target mRNA degradation. Cell *122*, 553–563.

Beckmann, K., Grskovic, M., Gebauer, F., and Hentze, M.W. (2005). A dual inhibitory mechanism restricts msl-2 mRNA translation for dosage compensation in Drosophila. Cell *122*, 529–540.

Bettinger, J.C., Lee, K., and Rougvie, A.E. (1996). Stage-specific accumulation of the terminal differentiation factor LIN-29 during Caenorhabditis elegans development. Development *122*, 2517–2527.

Bettinger, J.C., Euling, S., and Rougvie, A.E. (1997). The terminal differentiation factor LIN-29 is required for proper vulval morphogenesis and egg laying in Caenorhabditis elegans. Development *124*, 4333–4342.

Brabin, C., and Woollard, A. (2012). Finding a niche for seam cells? Worm *1*, 107–111.

Chang, H.M., Martinez, N.J., Thornton, J.E., Hagan, J.P., Nguyen, K.D., and Gregory, R.I. (2012). Trim71 cooperates with microRNAs to repress Cdkn1a expression and promote embryonic stem cell proliferation. Nat. Commun. *3*, 923.

Chatterjee, S., and Großhans, H. (2009). Active turnover modulates mature microRNA activity in Caenorhabditis elegans. Nature *461*, 546–549.

Chen, J., Lai, F., and Niswander, L. (2012). The ubiquitin ligase mLin41 temporally promotes neural progenitor cell maintenance through FGF signaling. Genes Dev. *26*, 803–815.

Chiu, S.C., Chung, H.Y., Cho, D.Y., Chan, T.M., Liu, M.C., Huang, H.M., Li, T.Y., Lin, J.Y., Chou, P.C., Fu, R.H., et al. (2014). Therapeutic potential of microRNA let-7: tumor suppression or impeding normal stemness. Cell Transplant. *23*, 459–469.

Dickinson, D.J., Pani, A.M., Heppert, J.K., Higgins, C.D., and Goldstein, B. (2015). Streamlined genome engineering with a self-excising drug selection cassette. Genetics *200*, 1035–1049.

Ding, X.C., and Großhans, H. (2009). Repression of C. elegans microRNA targets at the initiation level of translation requires GW182 proteins. EMBO J. *28*, 213–222.

Du, N., Kwon, H., Li, P., West, E.E., Oh, J., Liao, W., Yu, Z., Ren, M., and Leonard, W.J. (2014). EGR2 is critical for peripheral naïve T-cell differentiation and the T-cell response to influenza. Proc. Natl. Acad. Sci. USA *111*, 16484–16489.

Ecsedi, M., and Großhans, H. (2013). LIN-41/TRIM71: emancipation of a miRNA target. Genes Dev. *27*, 581–589.

Ecsedi, M., Rausch, M., and Großhans, H. (2015). The let-7 microRNA directs vulval development through a single target. Dev. Cell *32*, 335–344.

Edgar, R., Domrachev, M., and Lash, A.E. (2002). Gene Expression Omnibus: NCBI gene expression and hybridization array data repository. Nucleic Acids Res. *30*, 207–210.

Evans, T.C. (2006). Transformation and microinjection. WormBook, 1–15.

Fraser, A.G., Kamath, R.S., Zipperlen, P., Martinez-Campos, M., Sohrmann, M., and Ahringer, J. (2000). Functional genomic analysis of C. elegans chromosome I by systematic RNA interference. Nature *408*, 325–330.

Frøkjaer-Jensen, C., Davis, M.W., Hopkins, C.E., Newman, B.J., Thummel, J.M., Olesen, S.P., Grunnet, M., and Jorgensen, E.M. (2008). Single-copy insertion of transgenes in Caenorhabditis elegans. Nat. Genet. *40*, 1375–1383.

Frøkjær-Jensen, C., Davis, M.W., Ailion, M., and Jorgensen, E.M. (2012). Improved Mos1-mediated transgenesis in C. elegans. Nat. Methods *9*, 117–118.

Gibson, D.G., Young, L., Chuang, R.Y., Venter, J.C., Hutchison, C.A., 3rd, and Smith, H.O. (2009). Enzymatic assembly of DNA molecules up to several hundred kilobases. Nat. Methods *6*, 343–345.

Großhans, H., Johnson, T., Reinert, K.L., Gerstein, M., and Slack, F.J. (2005). The temporal patterning microRNA let-7 regulates several transcription factors at the larval to adult transition in C. elegans. Dev. Cell *8*, 321–330.

Harris, D.T., and Horvitz, H.R. (2011). MAB-10/NAB acts with LIN-29/EGR to regulate terminal differentiation and the transition from larva to adult in C. elegans. Development *138*, 4051–4062.

Hendriks, G.J., Gaidatzis, D., Aeschimann, F., and Großhans, H. (2014). Extensive oscillatory gene expression during C. elegans larval development. Mol. Cell *53*, 380–392.

Hinnebusch, A.G. (2005). Translational regulation of GCN4 and the general amino acid control of yeast. Annu. Rev. Microbiol. *59*, 407–450.

Ikeda, K., and Inoue, S. (2012). TRIM proteins as RING finger E3 ubiquitin ligases. Adv. Exp. Med. Biol. *770*, 27–37.

Jonas, S., and Izaurralde, E. (2015). Towards a molecular understanding of microRNA-mediated gene silencing. Nat. Rev. Genet. *16*, 421–433.

Joshi, P.M., Riddle, M.R., Djabrayan, N.J., and Rothman, J.H. (2010). Caenorhabditis elegans as a model for stem cell biology. Dev. Dyn. *239*, 1539–1554.

Katic, I., Xu, L., and Ciosk, R. (2015). CRISPR/Cas9 genome editing in Caenorhabditis elegans: evaluation of templates for homology-mediated repair and knock-ins by homology-independent DNA repair. G3 (Bethesda) *5*, 1649–1656.

Kühn, L.C. (2015). Iron regulatory proteins and their role in controlling iron metabolism. Metallomics *7*, 232–243.

Kwon, S.C., Yi, H., Eichelbaum, K., Föhr, S., Fischer, B., You, K.T., Castello, A., Krijgsveld, J., Hentze, M.W., and Kim, V.N. (2013). The RNA-binding protein repertoire of embryonic stem cells. Nat. Struct. Mol. Biol. *20*, 1122–1130.

Laslo, P., Spooner, C.J., Warmflash, A., Lancki, D.W., Lee, H.J., Sciammas, R., Gantner, B.N., Dinner, A.R., and Singh, H. (2006). Multilineage transcriptional priming and determination of alternate hematopoietic cell fates. Cell *126*, 755–766.

Le, N., Nagarajan, R., Wang, J.Y., Svaren, J., LaPash, C., Araki, T., Schmidt, R.E., and Milbrandt, J. (2005). Nab proteins are essential for peripheral nervous system myelination. Nat. Neurosci. *8*, 932–940.

Livak, K.J., and Schmittgen, T.D. (2001). Analysis of relative gene expression data using real-time quantitative PCR and the 2(-Delta Delta C(T)) Method. Methods *25*, 402–408.

Loedige, I., Gaidatzis, D., Sack, R., Meister, G., and Filipowicz, W. (2013). The mammalian TRIM-NHL protein TRIM71/LIN-41 is a repressor of mRNA function. Nucleic Acids Res. *41*, 518–532.

Loedige, I., Stotz, M., Qamar, S., Kramer, K., Hennig, J., Schubert, T., Löffler, P., Längst, G., Merkl, R., Urlaub, H., and Meister, G. (2014). The NHL domain of BRAT is an RNA-binding domain that directly contacts the hunchback mRNA for regulation. Genes Dev. *28*, 749–764.

Loedige, I., Jakob, L., Treiber, T., Ray, D., Stotz, M., Treiber, N., Hennig, J., Cook, K.B., Morris, Q., Hughes, T.R., et al. (2015). The crystal structure of the NHL domain in complex with RNA reveals the molecular basis of Drosophila brain-tumor-mediated gene regulation. Cell Rep. *13*, 1206–1220.

Löer, B., Bauer, R., Bornheim, R., Grell, J., Kremmer, E., Kolanus, W., and Hoch, M. (2008). The NHL-domain protein Wech is crucial for the integrin-cytoskeleton link. Nat. Cell Biol. *10*, 422–428.

Mason, D.A., Rabinowitz, J.S., and Portman, D.S. (2008). dmd-3, a doublesex-related gene regulated by tra-1, governs sex-specific morphogenesis in C. elegans. Development *135*, 2373–2382.

Medenbach, J., Seiler, M., and Hentze, M.W. (2011). Translational control via protein-regulated upstream open reading frames. Cell *145*, 902–913.

Merritt, C., Rasoloson, D., Ko, D., and Seydoux, G. (2008). 3′ UTRs are the primary regulators of gene expression in the C. elegans germline. Curr Biol *18*, 1476–1482.

Min, I.M., Pietramaggiori, G., Kim, F.S., Passegué, E., Stevenson, K.E., and Wagers, A.J. (2008). The transcription factor EGR1 controls both the proliferation and localization of hematopoietic stem cells. Cell Stem Cell *2*, 380–391.

Mitschka, S., Ulas, T., Goller, T., Schneider, K., Egert, A., Mertens, J., Brüstle, O., Schorle, H., Beyer, M., Klee, K., et al. (2015). Co-existence of intact stemness and priming of neural differentiation programs in mES cells lacking Trim71. Sci. Rep. *5*, 11126.

Nguyen, H.Q., Hoffman-Liebermann, B., and Liebermann, D.A. (1993). The zinc finger transcription factor Egr-1 is essential for and restricts differentiation along the macrophage lineage. Cell *72*, 197–209.

Rehfeld, F., Rohde, A.M., Nguyen, D.T., and Wulczyn, F.G. (2015). Lin28 and let-7: ancient milestones on the road from pluripotency to neurogenesis. Cell Tissue Res. *359*, 145–160.

Reinhart, B.J., Slack, F.J., Basson, M., Pasquinelli, A.E., Bettinger, J.C., Rougvie, A.E., Horvitz, H.R., and Ruvkun, G. (2000). The 21-nucleotide let-7 RNA regulates developmental timing in Caenorhabditis elegans. Nature *403*, 901–906.

Rougvie, A.E., and Ambros, V. (1995). The heterochronic gene lin-29 encodes a zinc finger protein that controls a terminal differentiation event in Caenorhabditis elegans. Development *121*, 2491–2500.

Rougvie, A.E., and Moss, E.G. (2013). Developmental transitions in C. elegans larval stages. Curr. Top. Dev. Biol. *105*, 153–180.

Rüegger, S., Miki, T.S., Hess, D., and Großhans, H. (2015). The ribonucleotidyl transferase USIP-1 acts with SART3 to promote U6 snRNA recycling. Nucleic Acids Res. *43*, 3344–3357.

Rybak, A., Fuchs, H., Hadian, K., Smirnova, L., Wulczyn, E.A., Michel, G., Nitsch, R., Krappmann, D., and Wulczyn, F.G. (2009). The let-7 target gene mouse lin-41 is a stem cell specific E3 ubiquitin ligase for the miRNA pathway protein Ago2. Nat. Cell Biol. *11*, 1411–1420.

Schindelin, J., Arganda-Carreras, I., Frise, E., Kaynig, V., Longair, M., Pietzsch, T., Preibisch, S., Rueden, C., Saalfeld, S., Schmid, B., et al. (2012). Fiji: an open-source platform for biological-image analysis. Nat. Methods *9*, 676–682.

Slack, F.J., Basson, M., Liu, Z., Ambros, V., Horvitz, H.R., and Ruvkun, G. (2000). The lin-41 RBCC gene acts in the C. elegans heterochronic pathway between the let-7 regulatory RNA and the LIN-29 transcription factor. Mol. Cell *5*, 659–669.

Spike, C.A., Coetzee, D., Eichten, C., Wang, X., Hansen, D., and Greenstein, D. (2014a). The TRIM-NHL protein LIN-41 and the OMA RNA-binding proteins antagonistically control the prophase-to-metaphase transition and growth of Caenorhabditis elegans oocytes. Genetics *198*, 1535–1558.

Spike, C.A., Coetzee, D., Nishi, Y., Guven-Ozkan, T., Oldenbroek, M., Yamamoto, I., Lin, R., and Greenstein, D. (2014b). Translational control of the oogenic program by components of OMA ribonucleoprotein particles in Caenorhabditis elegans. Genetics *198*, 1513–1533.

Tocchini, C., and Ciosk, R. (2015). TRIM-NHL proteins in development and disease. Semin. Cell Dev. Biol. *47-48*, 52–59.

Tocchini, C., Keusch, J.J., Miller, S.B., Finger, S., Gut, H., Stadler, M.B., and Ciosk, R. (2014). The TRIM-NHL protein LIN-41 controls the onset of developmental plasticity in Caenorhabditis elegans. PLoS Genet. *10*, e1004533.

Topilko, P., Schneider-Maunoury, S., Levi, G., Baron-Van Evercooren, A., Chennoufi, A.B., Seitanidou, T., Babinet, C., and Charnay, P. (1994). Krox-20 controls myelination in the peripheral nervous system. Nature *371*, 796–799.

Vella, M.C., Choi, E.Y., Lin, S.Y., Reinert, K., and Slack, F.J. (2004). The C. elegans microRNA let-7 binds to imperfect let-7 complementary sites from the lin-41 3'UTR. Genes Dev. *18*, 132–137.

Worringer, K.A., Rand, T.A., Hayashi, Y., Sami, S., Takahashi, K., Tanabe, K., Narita, M., Srivastava, D., and Yamanaka, S. (2014). The let-7/LIN-41 pathway regulates reprogramming to human induced pluripotent stem cells by controlling expression of prodifferentiation genes. Cell Stem Cell *14*, 40–52.

Wright, J.E., and Ciosk, R. (2013). RNA-based regulation of pluripotency. Trends Genet. *29*, 99–107.

Wright, J.E., Gaidatzis, D., Senften, M., Farley, B.M., Westhof, E., Ryder, S.P., and Ciosk, R. (2011). A quantitative RNA code for mRNA target selection by the germline fate determinant GLD-1. EMBO J *30*, 533–545.

Ye, J., and Blelloch, R. (2014). Regulation of pluripotency by RNA binding proteins. Cell Stem Cell *15*, 271–280.

STAR★METHODS

KEY RESOURCES TABLE

REAGENT or RESOURCE	SOURCE	IDENTIFIER
Antibodies		
Monoclonal mouse anti-FLAG M2-Peroxidase (HRP)	Sigma-Aldrich	Cat#A8592, RRID: AB_439702
Monoclonal mouse anti-Actin clone C4	Millipore	Cat#MAB1501, RRID: AB_2223041
Horseradish peroxidase-conjugated secondary antibody	GE Healthcare	Cat#NXA931, RRID: AB_772209
Chemicals, Peptides, and Recombinant Proteins		
StrepTag-TEV-LIN41_Filamin_NHL_Domain (*C. elegans*)	This study	N/A
Critical Commercial Assays		
ScriptSeq v2 RNA-Seq library preparation kit	Epicenter	Cat#SSV21124
Ribo-Zero rRNA Removal Kit	Epicenter	Cat#MRZH11124
TruSeq Small RNA Sample Preparation Kit	Illumina	Cat#RS-200-0012
Deposited Data		
Ribosome profiling and RNA sequencing data for wild-type run in parallel with *let-7(n2853)*	Hendriks et al., 2014	GEO: GSE52864 (GSM1277189-GSM1277198) and GEO GSE52905
Ribosome profiling and RNA sequencing data	This study	GEO: GSE80159
Raw microscopy image data related to main figures	This study	doi: 10.17632/wkcr5gb4t5.1 (Mendeley)
Experimental Models: Organisms/Strains		
C. elegans lines are listed in Table S4	N/A	N/A
Recombinant DNA		
Plasmids are listed in Table S5	N/A	N/A
Primers are listed in Tables S6 (qPCR) and S7 (EMSA probe generation)	N/A	N/A

CONTACT FOR REAGENT AND RESOURCE SHARING

Helge Großhans, Friedrich Miescher Institute for Biomedical Research, helge.grosshans@fmi.ch, will respond to request and provide reagents and information. Published research reagents from the FMI are shared with the academic community under a Material Transfer Agreement (MTA) having terms and conditions corresponding to those of the UBMTA (Uniform Biological Material Transfer Agreement).

EXPERIMENTAL MODEL AND SUBJECT DETAILS

C. elegans

The worm strains used in this study are listed in Table S4. The wild-type strain was Bristol N2. To synchronize worms, arrested L1 stage larvae were obtained by extracting embryos from gravid adults using a bleaching solution (30% (v/v) sodium hypochlorite (5% chlorine) reagent (Thermo Fisher Scientific; 419550010), 750 mM KOH). *let-7(n2853)* embryos were extracted from mothers grown at permissive temperature (15°C). Synchronized arrested L1 larvae (L1s) were obtained by hatching overnight in the absence of food, at room temperature in M9 buffer (42 mM Na_2HPO_4, 22 mM KH_2PO_4, 86 mM NaCl, 1 mM $MgSO_4$), plated on food and incubated at 25°C for the desired time (termed hours of development in the respective experiments). For ribosome profiling or RNA-IP experiments, L1s were plated on enriched peptone plates with *Escherichia coli* NA22 bacteria (Evans, 2006). For RNAi experiments, L1s were plated on RNAi-inducing NGM agar plates with *Escherichia coli* HT115 bacteria containing plasmids targeting the gene of interest (Ahringer, 2006).

METHOD DETAILS

Ribosome Profiling and Total RNA Sequencing

Ribosome profiling time course experiments were performed according to our detailed published protocol (Aeschimann et al., 2015). In brief, synchronized worms, grown on enriched peptone plates with NA22 bacteria, were harvested every two hours from 18 hr to 36 or 38 hr, respectively, of development at 25°C. Between 200,000 worms (earliest time points) and 100,000 worms (latest time points) were collected. Worm lysates of 11 absorbance units at 260 nm were prepared in a total volume of 385 μl and digested with 2 μl of RNaseI (100 Units/μl, Life Technologies; AM2295) for 1 hr at 23°C. Monosomes were purified using linear sucrose density gradients for the first time course experiment (wild-type and *let-7(n2853)* animals) and using size-exclusion chromatography for the second time course experiment (wild-type, *lin-41(xe11)* and *lin-41(xe11); let-7(n2853)* animals), as described in (Aeschimann et al., 2015). RPFs were obtained by separation of the monosomal RNA on Novex 15% (w/v) Polyacrylamide TBE-Urea Gels (Life Technologies; EC6885BOX) and extraction of 28-30 nt long RNAs. Library preparation was performed according to the TruSeq Small RNA Sample Preparation Kit (Illumina; RS-200-0012), adjusted as described in (Aeschimann et al., 2015). For total RNA sequencing, a sample of the input RNA (before the RNase digest) was extracted using Tri Reagent (Molecular Research Center; TR 118) according to the manufacturer's recommendations. To obtain ribosomal RNA (rRNA)-depleted total RNA, a DNase-treatment was performed with the RNase-Free DNase Set (QIAGEN; 79254) and the RNeasy MiniKit (QIAGEN; 74104), before using the Ribo-Zero rRNA Removal Kit (Epicenter; MRZH11124) to remove rRNA. Libraries were prepared with the ScriptSeq v2 RNA-Seq library preparation kit (Epicenter; SSV21124) and, like RPF libraries, sequenced on an Illumina HiSeq2000 machine. The data of the first wild-type animal time course, collected for the ribosome profiling experiment with wild-type and *let-7(n2853)* worms, was first published elsewhere (Hendriks et al., 2014), GEO: GSE52864 (GSM1277189-GSM1277198) and GEO: GSE52905. Data analysis is described in the relevant section below.

Construction of GFP Reporters

All reporters were constructed using the MultiSite Gateway Technology (Thermo Fisher Scientific) and the destination vector pCFJ150 (Frøkjaer-Jensen et al., 2008). First, promoters, 5′UTRs and 3′UTRs were amplified from *C. elegans* genomic DNA or ordered as gBlocks® Gene Fragments (Integrated DNA Technologies), before inserting them into Entry clones using the Gateway BP Clonase II Enzyme mix (Thermo Fisher Scientific; 11789020) or Gibson assembly (Gibson et al., 2009). PCR primer or gBlock sequences, cloning techniques and resulting Entry plasmids are listed in Table S5. Second, three entry plasmids were recombined with the pCFJ150 vector backbone (Gateway LR Clonase II Enzyme mix, Thermo Fisher Scientific; 11791020) to a plasmid with promoter, 5′UTR, GFP(PEST)-H2B coding sequence and 3′UTR. Third, transgenic worms were obtained by single-copy integration into the *ttTi5605* locus on chromosome II, following the published protocol for injection with low DNA concentration (Frøkjær-Jensen et al., 2012).

Confocal Imaging and RNA Extraction

Before subjecting worms to RNA extraction or confocal imaging, they were grown for 20 hr at 25°C on RNAi-inducing plates with HT115 bacteria, either containing the insert-less L4440 parental RNAi vector (denoted "mock RNAi") or an RNAi vector with an insert targeting *lin-41* (Fraser et al., 2000). For RNA extraction, worms were harvested and washed with M9 buffer and frozen in 1 mL of Tri Reagent at −80°C until further use. RNA was extracted according to the Tri Reagent manufacturer's protocol, following lysis of worms with five repeats of freeze and thaw cycles using liquid nitrogen and a heating block at 42°C. For confocal imaging, worms were mounted on a 2% (w/v) agarose pad with a drop of 10 mM levamisole solution, and imaged on a Zeiss LSM 700 confocal microscope driven by Zen 2012 Software. Before acquiring images of representative worms, the GFP signals for at least 10 worms were observed to verify that they were comparable among different worms in each worm line and for each condition. A second independent integrant line was obtained for each construct and examined to confirm results. Fluorescent and Differential Interference Contrast (DIC) images were acquired with a 40x/1.3 oil immersion objective (1024x1024 pixels, pixel size 156nm). Selections of representative regions and processing of images was performed with Fiji (Schindelin et al., 2012). Identical worm lines grown on mock or *lin-41* RNAi bacteria were imaged and processed with identical settings. In LIN41-depleted worms of the L3 stage used for imaging, nuclear GFP reporters driven from the *dpy-30* promoter accumulated in seam cell nuclei as well as in the surrounding hypodermal (hyp7) nuclei, while those driven from the *lin-29A* promoter only accumulated in hyp7 nuclei. The latter expression pattern was also observed for endogenously tagged LIN-29 during L3 stage. LIN-29 in wild-type worms accumulates in seam cells starting only in the L4 stage (Bettinger et al., 1996; data not shown).

RNA Co-immunoprecipitation (RIP)

RIP was performed with non-transgenic wild-type worms, wild-type worms expressing *flag::gfp::sart-3* (Rüegger et al., 2015) and *lin-41(n2914)* mutant worms expressing *flag::gfp::lin-41*. The transgene for expression of *flag::gfp::lin-41* was cloned using MultiSite Gateway Technology and single-copy integrated on chromosome II, as described for the construction of GFP reporters (primers and Entry plasmids are listed in Table S5). The transgenic line was outcrossed four times to the wild-type strain before crossing it into the *lin-41(n2914)* mutant background. Worms with transgenic expression of FLAG::GFP::LIN41 in the *lin-41(n2914)* mutant background were superficially wild-type, and did not show any of the *lin-41(n2914)* mutant phenotypes (sterility, lethality, dumpiness).

Worms were harvested as semi-synchronous L3/L4 stage populations, obtained by bleaching of gravid adults, followed by directly plating the extracted embryos on enriched peptone plates with NA22 bacteria and incubating them for approximately 30 hr at 25°C. Worm pellets of about 1 mL were lysed in extraction buffer (50 mM HEPES/KOH (pH 7.4 at 4°C), 150 mM KCl, 5 mM $MgCl_2$, 0.1% (v/v) Triton X-100, 10% (w/v) glycerol, 1 mM PMSF, 7 mg/ml cOmplete Protease Inhibitor Tablets (EDTA-free, Roche; 11873580001), 200 U/ml RNase inhibitor (e.g., SUPERase In RNase Inhibitor, Life Technologies; AM2696)), with mortar and pestle in the presence of liquid nitrogen (see also (Aeschimann et al., 2015)). Lysates were cleared by centrifugation at 12,000 g for 10 min at 4°C. Anti-FLAG IPs were performed by incubating 3 mg total protein with 30 μl of anti-FLAG M2 magnetic beads (Sigma–Aldrich; M8823) for 3 hr at 4°C on a rotating wheel. Beads were washed five times for five minutes in extraction buffer without protease and RNase inhibitors, before extracting the bound RNA by directly adding Tri Reagent to the beads. For each condition, five IPs were performed in parallel to increase the amount of recovered RNA. A sample of input RNA was extracted from an aliquot of remaining input lysate using Tri Reagent. Reverse transcription (see below) was performed with 900 ng of input RNA and with 50% of the IP RNA, respectively. (IP RNA was not quantified due to low amounts.) After RT-qPCR analysis, a relative enrichment ("re") in IP versus input was calculated for each measured mRNA, separately for LIN41 IP, SART-3 IP and wild-type IP: re = 2^(CT (input) - CT (IP)). Fold enrichments compared to mock IP were then calculated by dividing LIN41 and SART-3 IP "re" values by the wild-type IP "re" values.

RT-qPCR

Reverse transcription was performed with the ImpromII Reverse Transcription System (Promega; A3800), according to the manufacturer's protocol, with 900 ng RNA (except for RNA from RIPs) and random primers (Promega; C1181). Using SYBR Green PCR Master Mix (Thermo Fisher Scientific; 4309155), qPCR was performed on a StepOnePlus Real-Time PCR System (Thermo Fisher Scientific) with the primers listed in Table S6. For comparing mRNA levels of the GFP reporters or of GFP-3xFLAG-tagged *lin-29*, grown on *lin-41* or mock RNAi bacteria, GFP mRNA fold changes were calculated with the $2^{-\Delta\Delta CT}$ Method (Livak and Schmittgen, 2001), using *act-1* as an internal control mRNA and the mock RNAi condition as calibrator.

Western Blotting

Worms were grown for 20 hr at 25°C on RNAi-inducing plates, as described above for confocal imaging and RNA extraction. Lysates were made by boiling (5 min, 95°C) and sonication in SDS lysis buffer (63 mM Tris-HCl (pH 6.8), 5 mM DTT, 2% SDS, 5% sucrose) and cleared by centrifugation, before separating proteins by SDS-PAGE (loading: 50 μg protein extract per well) and transferring them to PVDF membranes by semi-dry blotting. The following antibodies were used: Monoclonal mouse anti-FLAG M2-Peroxidase (HRP) (Sigma-Aldrich; A8592, dilution: 1:1,000). Monoclonal mouse anti-Actin clone C4 (Millipore; MAB1501, dilution 1:10,000). A horseradish peroxidase-conjugated secondary antibody (NXA931), ECL Western Blotting Detection Reagents and an ImageQuant LAS 4000 chemiluminescence imager (all from GE Healthcare) were used for signal generation and detection, respectively.

Tagging of Endogenous *lin-29* by CRISPR-Cas9

Wild-type worms were injected with a mix of 50 ng/μl pIK155, 100 ng/μl of pIK198 with a cloned sgRNA (atattatttatcagtgattg), 2.5 ng/μl pCFJ90, 5 ng/μl pCFJ104 and 10 ng/μl pDD282 with cloned homology arms, as described in (Dickinson et al., 2015; Katic et al., 2015). The plasmid for homologous recombination was prepared by restriction digest of pDD282 with ClaI and SpeI, followed by a 3-fragment Gibson assembly reaction (Gibson et al., 2009) with two gBlocks® Gene Fragments (Integrated DNA Technologies), as described in Table S5. Recombinants were isolated according to the protocol by Dickinson et al. (Dickinson et al., 2015), verified by DNA sequencing and outcrossed three times. Two independent worm lines were obtained and characterized.

Electrophoretic Mobility Shift Assay

Radioactively labeled probes for EMSAs were transcribed from PCR products with T3 RNA polymerase. Templates for probe synthesis were generated by PCR with an extended phage T3 RNA polymerase promoter (AATTAACCCTCACTAAAGGGAGAA) appended to the 5′end of the 5′primer, and gel-purified (primers are listed in Table S7). Labeled probes were transcribed in 3 μl reactions containing 0.5 μl template, 1.5 μl $^{\alpha}$P32 UTP (3 μM) (Hartmann Analytic), 0.6 μl 5x transcription buffer (Promega), 0.4 μl T3 polymerase (Promega), 0.2 μl RNasin (Promega), 2.5 mM rATP, rGTP and rCTP, and 0.025 mM rUTP (Roche) at 37°C for 3 hr. The reaction was stopped by adding 40 μl Tris-EDTA buffer (10 mM Tris-HCl (pH 8.0), 1 mM EDTA) containing 30% glycerol and ~0.01% Bromophenol Blue. The C-terminal part of LIN41 containing the Filamin and NHL domains was produced as a Strep-tagged fusion protein in Sf9 insect cells using the baculovirus expression system (Invitrogen). The recombinant protein was affinity-purified by the Strep tag using Macroprep Strep-Tactin beads (IBA) according to the manufacturer's instruction. Protein was concentrated using ultra centrifugal filters (Amicon) and stored in aliquots at −80°C.

1 μl of 5 μM protein was pre-incubated with 4 μl of 2x gel-shift buffer (20 mM HEPES pH 8, 100 mM KCl, 200 mM NaCl, 0.2 mM EDTA, 20 mM DTT, 2 mM $MgCl_2$, 2 mM $CaCl_2$, 0.2 mM $ZnSO_4$, 60% glycerol, 500 μg/ml heparin, 50 μg/ml *E. coli* tRNA). The reaction was made up to 7 μl with sterile water, incubated for 10 min at room temperature, following which 1 μl of RNA probe (~2 nM, ~10^5 cpm) was added. The reaction was incubated for 20 min and loaded onto the gel, electrophoresed at 25 mA, dried, and auto-radiographed. The cathode buffer was 50 mM glycine, 6 mM TRIS, 0.2 mM EDTA, pH 8), the stacking gel was 25 mM TRIS pH 6.8, 3% 19:1 acrylamide:bisacrylamide, the resolving gel was 0.5 X TBE (45 mM Tris-borate pH 8.3, 1 mM EDTA), 6% 19:1 acrylamide:bisacrylamide, and the anode buffer was 0.5X TBE. For competition gel-shift assays, increasing amounts of cold (unlabeled) competitor RNA

was added to the gel-shift reaction described above. 12 nM, 60 nM or 300 nM of cold RNA was incubated with LIN-41_Fil_NHL protein in 1x gel-shift buffer for 20 min, following which 1 μl of RNA probe (~2 nM, ~10^5 cpm) was added. The reaction was further incubated for 20 min and loaded onto the gel.

QUANTIFICATION AND STATISTICAL ANALYSES

Ribosome Profiling and RNA-Seq Data Analysis

RPF as well as RNA-seq data were processed and normalized as previously described (Hendriks et al., 2014), with separate normalizations for each batch of time course experiments. In all figures, expression levels are depicted as normalized $\log_2$ read counts. Before $\log_2$ transformation, a pseudocount of 8 was added to minimize large differences in expression caused by genes with a low number of read counts. Zero read counts thus result in a $\log_2$ read count of $\log_2(8) = 3$. The comparison of gene expression changes in the different mutants was performed with normalized $\log_2$ RPF counts, averaged for the five time points at 28, 30, 32, 34, and 36 hr (*lin-41* repression plateau). Consistently dysregulated genes at the RPF level in *let-7(n2853)* and *lin-41(xe11)* as compared to wild-type animals were identified based on the scatterplot depicted in Figure 1D. To compensate for the lower extent of *lin-41* dysregulation relative to the *let-7(n2853)* situation, we amplified the $\log_2$ fold changes in the *lin-41(xe11)* mutant by a factor of 1.5 for further processing. We first selected the up- and downregulated genes in the two mutants by requiring an average (adjusted) $\log_2$ fold change of at least 0.85. Second, to remove genes that were selected because they were mainly dysregulated in only one of the two mutants, we excluded genes with more than ± 30 degree angular deviation from the diagonal. To examine temporal changes of the selected up- and downregulated genes, the RPF read profiles were visually examined to determine the earliest developmental time point in which each gene was clearly and consistently dysregulated in all of the three mutant animals (*let-7(n2853)*, *lin-41(xe11)* and *lin-41(xe11); let-7(n2853)*, Table S3). To analyze RPF and RNA-seq data for the different exons of the *lin-29* gene, reads were counted in each of the 11 exons of the *lin-29A* (W03C9.4a) isoform separately (Rougvie and Ambros, 1995). Reads were normalized as above, with each exon treated as if it were a separate gene. In order to analyze the expression pattern of the exons specific to *lin-29A* versus all other exons (Figure 4B), the normalized reads for exons 1-4 and for exons 5-11 were summed up before addition of a pseudocount of 8 and $\log_2$ transformation. In order to analyze the expression changes for each separate exon during the *lin-41* repression plateau (Figure 4A), normalized RPF and mRNA read counts were summed up for the five time points at 28, 30, 32, 34 and 36 hr. Next, the read sums were $\log_2$ transformed, after addition of a pseudocount of 2. (Here, we chose a lower pseudocount to be able to visualize fold changes even with low read numbers per exon.) The fold downregulation for RPF and mRNA reads, respectively, was then quantified as differences in $\log_2$ read sums between wild-type and mutant. The non-coding exon 1 (pure 5′UTR sequence, no ATG start codon present) was included in this analysis, because we observed RPFs mapping to it, although at lower numbers than to coding exons. RPF reads in 5′UTRs have been observed in many studies, including our own metagene analysis (Aeschimann et al., 2015). While the nature of the reads mapping to *lin-29* exon 1 is unclear to us, they only accumulate in the absence of LIN41.

RT-qPCR Analysis

All RT-qPCR data are depicted as the mean of n = 3 or n = 4 biological replicates, with error bars representing ± s.e.m. In this study, a biological replicate is defined as an independently grown worm population, before extraction of embryos from gravid adults to obtain synchronized or semi-synchronized populations of worms (see EXPERIMENTAL MODEL AND SUBJECT DETAILS). The exact values of n are indicated in the figure legends.

For all reporter experiments, GFP or *lin-41* mRNA fold changes are calculated using the $2^{-\Delta\Delta CT}$ Method (Livak and Schmittgen, 2001), with *act-1* as an internal control mRNA and mock RNAi condition as calibrator. For each measured mRNA in each RNA-IP, a relative enrichment (“re”) in IP versus input is calculated: re = 2^(CT (input) - CT (IP)). The depicted fold enrichments compared to mock IP are calculated by dividing LIN41 and SART-3 IP “re” values by the wild-type IP “re” values. See also the relevant sections in the METHOD DETAILS.

DATA AND SOFTWARE AVAILABILITY

All ribosome profiling and RNA-sequencing data generated in this study have been deposited in the NCBI Gene Expression Omnibus (Edgar et al., 2002) under GEO: GSE80159. The wild-type time course data used for the comparison to *let-7(n2853)* have been previously deposited under accession numbers GEO: GSE52864 (GSM1277189-GSM1277198) and GEO: GSE52905. Raw microscopy image data for all main figures have been deposited at Mendeley, doi: 10.17632/wkcr5gb4t5.1.